



# Fragment-based drug discovery and biological evaluation of novel cannabinol-based inhibitors of oxytosis/ferroptosis for neurological disorders

Zhibin Liang<sup>a,\*</sup>, Alec Candib<sup>b</sup>, David Soriano-Castell<sup>a</sup>, Wolfgang Fischer<sup>a</sup>, Kim Finley<sup>b</sup>, Pamela Maher<sup>a,\*\*</sup>

<sup>a</sup> Cellular Neurobiology Laboratory, The Salk Institute for Biological Studies, 10010 North Torrey Pines Road, La Jolla, CA, 92037, United States

<sup>b</sup> Shiley Bioscience Center, San Diego State University, 5500 Campanile Drive, San Diego, CA, 92182, United States

## ARTICLE INFO

### Keywords:

Cannabinoid  
Drug discovery  
Neurotherapeutic  
Oxytosis/ferroptosis  
Mitochondrial dysfunction  
Neurological disorder  
Traumatic brain injury  
*Drosophila*

## ABSTRACT

The oxytosis/ferroptosis regulated cell death pathway is an emerging field of research owing to its pathophysiological relevance to a wide range of neurological disorders, including Alzheimer's and Parkinson's diseases and traumatic brain injury. Developing novel neurotherapeutics to inhibit oxytosis/ferroptosis offers exciting opportunities for the treatment of these and other neurological diseases. Previously, we discovered cannabinol (CBN) as a unique, potent inhibitor of oxytosis/ferroptosis by targeting mitochondria and modulating their function in neuronal cells. To further elucidate which key pharmacophores and chemical space are essential to the beneficial effects of CBN, we herein introduce a fragment-based drug discovery strategy in conjunction with cell-based phenotypic screens using oxytosis/ferroptosis to determine the structure-activity relationship of CBN. The resulting information led to the development of four new CBN analogs, CP1-CP4, that not only preserve the sub-micromolar potency of neuroprotection and mitochondria-modulating activities seen with CBN in neuronal cell models but also have better druglike properties. Moreover, compared to CBN, the analog CP1 shows improved *in vivo* efficacy in the *Drosophila* model of mild traumatic brain injury. Together these studies identify the key molecular scaffolds of cannabinoids that contribute to neuroprotection against oxytosis/ferroptosis. They also highlight the advantageous approach of combining *in vitro* cell-based assays and rapid *in vivo* studies using *Drosophila* models for evaluating new therapeutic compounds.

## 1. Introduction

Neurological disorders, including Alzheimer's (AD), Parkinson's (PD), and Huntington's diseases (HD), as well as traumatic brain injury (TBI) affect millions of people worldwide [1]. These disorders are highly devastating conditions that cause progressive brain impairment and cognitive decline with often fatal consequences. Neurological disorders place an enormous burden on healthcare systems and their impact on society in general will continue to rise over the coming decades as the aging population increases throughout the world [1]. To date, there are no drugs for any of these conditions that are disease modifying in the sense that they prevent, cure, or slow down the progression of the neuropathological process [2,3]. This is due, at least in part, to the lack of a full understanding of the fundamental origins of these neurological

disorders [2].

Mitochondria are the primary source of energy in cells, and they execute complex and crucial tasks in the central nervous system (CNS) to keep the brain functioning properly. Growing evidence indicates that mitochondrial inefficiency and dysfunction occur in the aging brain and are one of the pathophysiological changes associated with neurological disorders [4]. Therefore, developing neurotherapeutics by targeting mitochondria to treat neurological disorders is highly attractive [5,6].

The oxytosis/ferroptosis regulated cell death pathway recapitulates many features of mitochondrial dysfunction associated with the aging brain and has emerged as a potential key mediator of neurological disorders [7,8]. It has thus been proposed that the oxytosis/ferroptosis pathway could be used to identify novel drug candidates that act by preserving mitochondrial function [9,10].

Using cell-based phenotypic assays in the context of oxytosis/

\* Corresponding author.

\*\* Corresponding author.

E-mail addresses: [zliang@salk.edu](mailto:zliang@salk.edu) (Z. Liang), [pmaher@salk.edu](mailto:pmaher@salk.edu) (P. Maher).

<https://doi.org/10.1016/j.redox.2024.103138>

Received 14 February 2024; Received in revised form 25 March 2024; Accepted 26 March 2024

Available online 29 March 2024

2213-2317/© 2024 The Authors. Published by Elsevier B.V. This is an open access article under the CC BY-NC-ND license (<http://creativecommons.org/licenses/by-nc-nd/4.0/>).

Abbreviations			
AD	Alzheimer's disease	OCR	oxygen consumption rate
PD	Parkinson's disease	MI	mortality index
HD	Huntington's disease	NMR	nuclear magnetic resonance
TBI	traumatic brain injury	HR-MS	high-resolution mass spectrometry
CNS	central nervous system	LU	left unit
mt	mitochondria	CU	central unit
SAR	structure-activity relationship	RU	right unit
ETC	electron transport chain	CBN	cannabinol
OXPPOS	oxidative phosphorylation	THC	tetrahydrocannabinol
ROS	reactive oxygen species	CBD	cannabidiol
LPO	lipid peroxidation	FCCP	carbonyl cyanide-4-(trifluoromethoxy)phenylhydrazone
RTA	radical-trapping antioxidant	MTT	3-(4,5-dimethylthiazol-2-yl)-2,5-diphenyltetrazolium bromide
CB1/CB2	cannabinoid receptors 1 and 2	EC <sub>50</sub>	half maximal effective concentration
A $\beta$	amyloid beta peptide	IC <sub>50</sub>	half maximal inhibitory concentration
APP	amyloid precursor protein	LC <sub>50</sub>	half maximal lethal concentration
ATP	adenosine triphosphate	FBDD	fragment-based drug discovery

ferroptosis, we recently screened libraries of medicinal phytocannabinoids including  $\Delta^9$ -tetrahydrocannabinol (THC), cannabidiol (CBD), and cannabinol (CBN) from the *Cannabis* plant, with the goal of identifying new natural product-based drug candidates that preserve mitochondrial function [11,12]. We discovered that cannabinol (CBN), a non-psychoactive phytocannabinoid, is a novel and potent neuroprotector that not only protects neurons from oxytosis/ferroptosis in a manner that is dependent on mitochondria, but it does so independently of cannabinoid CB1/CB2 receptors [12]. Specifically, CBN targets mitochondria and maintains mitochondrial homeostasis in neuronal cells [12]. Thus, CBN is an excellent lead compound derived from the *Cannabis* plant with high therapeutic potential and so it was selected for advancement into the lead optimization process of our drug discovery program.

To better understand the roles of the different pharmacophoric elements of CBN that are required for the inhibition of oxytosis/ferroptosis and mitochondrial modulation, we herein report a fragment-based drug discovery (FBDD) strategy [13] that exploits insights into the structure-activity relationship (SAR) of CBN. By applying this valuable information, we designed and synthesized four new analogs of CBN with improved physiochemical and CNS druglike properties. The neuroprotective activities and phenotypic profiles of each analog were evaluated using *in vitro* cell culture neural toxicity models and *in vivo* efficacy was assessed in the *Drosophila* model of mild traumatic brain injury (mTBI). Interestingly, although most of the analogs were highly protective in our *in vitro* cell culture neuroprotection assays, one of the analogs stood out as having beneficial effects in a *Drosophila* model of mTBI.

## 2. Material and methods

**Chemicals and Reagents.** All solvents and reagents were purchased from commercial sources and were used without further purification. Analytical scale quantities of CBN, CBD, THC standards, other natural and synthetic cannabinoids, and STY-BODIPY (Cat# 27089) were from Cayman Chemical (Ann Arbor, MI). Preparative scale quantities of CBN, CP1, CP2, CP3, and CP4 were synthesized in-house. Olivetol, 5-(1,1-dimethylheptyl)resorcinol, citral, but-2-enal, 3-methylbut-2-enal, *n*-butylamine, ethyl acetate, petroleum ether, toluene, glutamate, RSL3, erastin, and ferrostatin-1 were from Sigma-Aldrich (Saint Louis, MO). Phenol, catechol, hydroquinone, phloroglucinol, pyrogallol, hydroxyquinol, resorcinol, 5-methylresorcinol, 5-ethyl-1,3-benzenediol, 5-propylbenzene-1,3-diol, 5-butylresorcinol, 5-heptylresorcinol, 5-pentadecylresorcinol, 5-butoxybenzene-1,3-diol, 5-(pentylxy)benzene-

1,3-diol, 4-butylresorcinol, 4-hexylresorcinol, 4-butylbenzene-1,2-diol, 2-methylbenzene-1,4-diol, 2-*tert*-butylbenzene-1,4-diol, 4-propylphenol, 4-pentylphenol, 4-heptylphenol, 3-propylphenol, 3-pentylphenol, *n*-butane, *n*-pentane, *n*-hexane, *n*-heptane, *n*-octane, 2-methyloctane, *p*-cymene, *p*, $\alpha$ , $\alpha$ -trimethylbenzyl alcohol, 2-(*p*-tolyl)propan-2-amine, linalool, limonene,  $\alpha$ -terpineol, TLC plates, HyperSep silica column (Cat# 60108–712), MitoSOX Red Mitochondrial Superoxide Indicator (Cat# M36008), and C11-BODIPY Lipid Peroxidation Sensor (Cat# D3861) were from Thermo Fisher Scientific (Waltham, MA). Liposomes of egg-PC (Cat# 840051P) was from Avanti Polar Lipids Inc (Birmingham, AL). V-70 (Cat# 001–70078) was from Fujifilm Wako, Japan. Seahorse XFe96 FluxPak (Cat# 102416), Seahorse XF Cell Mito Stress Test Kit (Cat# 103015), and Seahorse XF Real-Time ATP Rate Assay Kit (Cat# 103592) were from Agilent Technologies (Santa Clara, CA).

**General Instrumental Analysis.** Optical absorbance and fluorescence were measured on a SpectraMax M5 Multi-Mode microplate reader (Molecular Devices, San Jose, CA).

**Microscopy.** Brightfield and phase contrast microscopic images were acquired on an IX51 inverted microscope (Olympus Corporation, Tokyo, Japan) with an INFINITY3 monochrome CCD camera (Teledyne Lumenera, Ontario, Canada). Image processing and analysis were performed with ImageJ/Fiji.

**Mass Spectrometry (MS).** High-resolution mass spectrometric data were obtained on a Thermo Q-Exactive Quadrupole-Orbitrap mass spectrometer in positive mode. Samples were diluted with a 1:1 mixture of methanol and water containing 0.1% formic acid and then introduced by direct electrospray infusion. Accurate masses of all analytes were obtained from the pseudo-molecule  $[M+H]^+$  and were within 5 ppm mass error. Full MS scans were recorded for the 150–750 *m/z* range. MS/MS fragmentation was achieved by higher-energy collisional dissociation (HCD) at normalized collision energy settings between 10 and 30%.

**Nuclear Magnetic Resonance (NMR).** <sup>1</sup>H, <sup>13</sup>C and 2D NMR data were collected at 298 K on a 600 MHz Bruker Avance III spectrometer fitted with a 1.7 mm triple resonance cryoprobe with z-axis gradients using TopSpin 3.6.0. NMR spectra were referenced to the residual solvent signal ( $\delta_H$  7.26,  $\delta_C$  77.2 for chloroform-*d*) with chemical shifts reported in  $\delta$  units (ppm). Resonance multiplicities are denoted s, d, t, q, m, and br for singlet, doublet, triplet, quartet, multiplet, and broad, respectively. 2D HSQC and HMBC NMR spectra were collected using modified versions of the Bruker pulse sequences hsqcedetgpsisp2.3 and hmbcctetgpl3ndsp, which incorporated an ASAP module to enable faster data acquisition. Spectral widths were 12 ppm for the <sup>1</sup>H dimensions, 160 ppm for the HSQC <sup>13</sup>C dimension and 250 ppm for the HMBC <sup>13</sup>C dimension. For the HSQC spectra 8 scans and 256 *t*<sub>1</sub> increments were

used. For the HMBC spectra 32 scans and 512  $t_1$  increments were used. Spectra were analyzed using Mnova.

**Fragment-Based Drug Discovery (FBDD).** Each fragment compound is chemically simple and most of the substructures are commercially available. Therefore, a series of fragment chemicals with different variants of the substructures were assembled and screened in our cell-based phenotypic screening assays in the context of oxytosis/ferroptosis. Specifically, for the left unit (LU), monoterpenoids with different functional groups and/or double-bond substitutions as well as ring arrangements were screened. For the central unit (CU), benzene rings with different hydroxyl group substitutions were screened. For the right unit (RU), different lengths, with or without branches, of the aliphatic hydrocarbon chains were examined.

After a number of fragment chemicals were screened, the SAR, basic chemical building blocks, and pharmacophores were assessed to determine which, if any, were active alone. This information was then used to identify the most active and viable substructure for each fragment. Combinations of substructures were used to form optimized CBN analogs through organic synthesis. The new CBN analogs were further evaluated for their physicochemical properties as well as their potency and efficacy in the *in vitro* and *in vivo* assays.

**In Silico ADME Prediction.** SwissADME tool (Swiss Institute of Bioinformatics, <http://www.swissadme.ch/>) was used to compute physicochemical descriptors and predict ADME parameters, pharmacokinetic properties, and the druglike nature of small molecules to support drug discovery [14].

**Total Synthesis of CP1 (2,2-dimethyl-7-(2-methyloctan-2-yl)-2H-chromen-5-ol).** To a stirred solution of 5-(1,1-dimethylheptyl)resorcinol (0.50 g, 2.1 mmol), 3-methylbut-2-enal (231  $\mu$ L, 2.75 mmol), and *n*-butylamine (201  $\mu$ L, 2.75 mmol) were added in toluene (50 mL). The mixture was refluxed for 6 h, and then cooled to room temperature. The reaction solution was evaporated to dryness with a rotatory evaporator. The residue was reconstituted in 5% ethyl acetate/petroleum ether and then eluted on a HyperSep silica column (10 g) using the same solvents to give CP1 as a yellow oil (0.54 g, 1.8 mmol, 85% total yield). The identity and purity of CP1 were confirmed by high-resolution NMR and mass spectrometry analyses.

Compound Characterization:  $^1\text{H}$  NMR (600 MHz,  $\text{CDCl}_3$ )  $\delta$  6.63 (d,  $J = 9.9$  Hz, 1H), 6.43 (d,  $J = 1.8$  Hz, 1H), 6.32 (d,  $J = 1.8$  Hz, 1H), 5.56 (d,  $J = 9.9$  Hz, 1H), 1.54–1.49 (m, 2H), 1.46 (s, 6H), 1.26 (m, 2H), 1.21 (s, 6H), 1.21–1.19 (m, 4H), 1.08 (m, 2H), 0.87 (t,  $J = 7.2$  Hz, 3H).  $^{13}\text{C}$  NMR (75 MHz,  $\text{CDCl}_3$ )  $\delta$  153.3, 152.1, 150.1, 128.4, 116.4, 107.1, 106.9, 105.9, 76.0, 44.4, 37.7, 31.8, 30.0, 28.8, 28.8, 27.8, 27.8, 24.6, 22.6, 14.1. HR-MS  $m/z$   $[\text{M}+\text{H}]^+$  303.2313 (calculated for  $\text{C}_{20}\text{H}_{31}\text{O}_2^+$ , 303.2324,  $-3.6$  ppm error). The purity of CP1 was over 95% as determined by quantitative NMR analysis.

**Total Synthesis of CP2 (2-methyl-7-(2-methyloctan-2-yl)-2H-chromen-5-ol).** To a stirred solution of 5-(1,1-dimethylheptyl)resorcinol (0.50 g, 2.1 mmol), but-2-enal (193  $\mu$ L, 2.75 mmol), and *n*-butylamine (201  $\mu$ L, 2.75 mmol) were added in toluene (50 mL). The mixture was refluxed for 6 h, and then cooled to room temperature. The reaction solution was evaporated to dryness with a rotatory evaporator. The residue was reconstituted in 5% ethyl acetate/petroleum ether and then eluted on a HyperSep silica column (10 g) using the same solvents to give CP2 as a yellow oil (0.52 g, 1.8 mmol, 87% total yield). The identity and purity of CP2 were confirmed by high-resolution NMR and mass spectrometry analyses.

Compound Characterization:  $^1\text{H}$  NMR (600 MHz,  $\text{CDCl}_3$ )  $\delta$  6.70 (dd,  $J = 9.8, 1.9$  Hz, 1H), 6.44 (s, 1H), 6.34 (s, 1H), 5.59 (dd,  $J = 9.8, 3.2$  Hz, 1H), 4.97 (dq,  $J = 3.2, 6.8$  Hz, 1H), 1.55–1.50 (m, 2H), 1.48 (d,  $J = 6.8$  Hz, 3H), 1.26 (m, 2H), 1.21 (s, 6H), 1.21–1.19 (m, 4H), 1.08 (m, 2H), 0.87 (t,  $J = 7.2$  Hz, 3H).  $^{13}\text{C}$  NMR (75 MHz,  $\text{CDCl}_3$ )  $\delta$  154.1, 152.2, 151.1, 124.4, 118.4, 107.7, 106.5, 106.2, 71.3, 44.7, 37.8, 31.8, 30.1, 28.7, 28.7, 24.7, 22.7, 21.1, 14.1. HR-MS  $m/z$   $[\text{M}+\text{H}]^+$  289.2155 (calculated for  $\text{C}_{19}\text{H}_{29}\text{O}_2^+$ , 289.2168,  $-4.3$  ppm error). The purity of CP2 was over 95% as determined by quantitative NMR analysis.

**Total Synthesis of CP3 (2,2-dimethyl-7-pentyl-2H-chromen-5-ol).** To a stirred solution of olivetol (0.5 g, 2.7 mmol), 3-methylbut-2-enal (231  $\mu$ L, 2.75 mmol), and *n*-butylamine (201  $\mu$ L, 2.75 mmol) were added in toluene (50 mL). The mixture was refluxed for 6 h, and then cooled to room temperature. The reaction solution was evaporated to dryness with a rotatory evaporator. The residue was reconstituted in 5% ethyl acetate/petroleum ether and then eluted on a HyperSep silica column (10 g) using the same solvents to give CP3 as a yellow oil (0.62 g, 2.5 mmol, 91% total yield). The identity and purity of CP3 were confirmed by high-resolution NMR and mass spectrometry analyses.

Compound Characterization:  $^1\text{H}$  NMR (600 MHz,  $\text{CDCl}_3$ )  $\delta$  6.64 (d,  $J = 9.9$  Hz, 1H), 6.28 (s, 1H), 6.20 (s, 1H), 5.53 (d,  $J = 9.9$  Hz, 1H), 2.44 (t,  $J = 7.9$  Hz, 2H), 1.57 (m, 2H), 1.43 (s, 6H), 1.33–1.24 (m, 4H), 0.91 (m, 3H).  $^{13}\text{C}$  NMR (75 MHz,  $\text{CDCl}_3$ )  $\delta$  153.5, 151.4, 144.7, 127.9, 116.7, 108.9, 108.2, 107.3, 76.0, 35.9, 31.5, 30.6, 27.7, 27.7, 22.5, 14.0. HR-MS  $m/z$   $[\text{M}+\text{H}]^+$  247.1687 (calculated for  $\text{C}_{16}\text{H}_{23}\text{O}_2^+$ , 247.1698,  $-4.5$  ppm error). The purity of CP3 was over 95% as determined by quantitative NMR analysis.

**Total Synthesis of CP4 (2-methyl-7-pentyl-2H-chromen-5-ol).** To a stirred solution of olivetol (0.5 g, 2.7 mmol), but-2-enal (193  $\mu$ L, 2.75 mmol), and *n*-butylamine (201  $\mu$ L, 2.75 mmol) were added in toluene (50 mL). The mixture was refluxed for 6 h, and then cooled to room temperature. The reaction solution was evaporated to dryness with a rotatory evaporator. The residue was reconstituted in 5% ethyl acetate/petroleum ether and then eluted on a HyperSep silica column (10 g) using the same solvents to give CP4 as a yellow oil (0.58 g, 2.5 mmol, 92% total yield). The identity and purity of CP4 were confirmed by high-resolution NMR and mass spectrometry analyses.

Compound Characterization:  $^1\text{H}$  NMR (600 MHz,  $\text{CDCl}_3$ )  $\delta$  6.79 (dd,  $J = 10.0, 2.1$  Hz, 1H), 6.38 (d,  $J = 2.3$  Hz, 1H), 6.26 (d,  $J = 2.3$  Hz, 1H), 5.61 (dd,  $J = 10.0, 3.4$  Hz, 1H), 4.98 (m, 1H), 2.47 (t,  $J = 7.7$  Hz, 2H), 1.59 (m, 2H), 1.49 (d,  $J = 7.7$  Hz, 3H), 1.41–1.28 (m, 4H), 0.95 (m, 3H).  $^{13}\text{C}$  NMR (75 MHz,  $\text{CDCl}_3$ )  $\delta$  153.8, 151.4, 144.8, 123.9, 118.4, 108.7, 108.6, 108.1, 71.3, 35.9, 31.4, 30.6, 22.5, 20.8, 14.0. HR-MS  $m/z$   $[\text{M}+\text{H}]^+$  233.1531 (calculated for  $\text{C}_{15}\text{H}_{21}\text{O}_2^+$ , 233.1542,  $-4.5$  ppm error). The purity of CP4 was over 95% as determined by quantitative NMR analysis.

**Cell Culture.** HT22 mouse hippocampal nerve cells and MC65 human nerve cells were cultured in high-glucose Dulbecco's modified Eagle's medium (DMEM) (Invitrogen, Cat# 11995065, Carlsbad, CA) supplemented with 10% fetal bovine serum (FBS) (Invitrogen, Carlsbad, CA) and 1% antibiotics including penicillin and streptomycin (Invitrogen Cat# 10378016, Carlsbad, CA). Cell cultures were incubated at 37 °C in a fully humidified atmosphere containing 10%  $\text{CO}_2$ .

**Oxytosis Assay.** The assay procedure was previously described [15]. HT22 cells were seeded at 3,000 cells/well in 96-well tissue culture plates in DMEM plus 10% FBS and 1% antibiotics. After 24 h of plating, the cells were pretreated with different concentrations of the test compounds or a vehicle control for 1 h followed by addition of 5 mM glutamate to initiate the cell death cascade. After 16 h of treatment, cell viability was measured by the 3-(4,5-dimethylthiazol-2-yl)-2,5-diphenyltetrazolium bromide (MTT) assay. Optical absorbance was measured at 570 nm on a SpectraMax M5 microplate reader. Samples were analyzed in four independent replicates. Results are presented as % neuroprotection or half maximal effective concentrations ( $\text{EC}_{50}$ ). Results were verified by visual inspection of the cells under a microscope.

**Ferroptosis Assay.** The assay procedure was previously described [15]. HT22 cells were seeded at 3,000 cells/well in 96-well tissue culture plates in DMEM plus 10% FBS and 1% antibiotics. After 24 h of plating, the cells were pretreated with different concentrations of test compounds or a vehicle control for 1 h followed by addition of 50–100 nM RSL3 or 500 nM erastin to induce the cell death cascade. After 16 h of treatment, cell viability was measured by the MTT assay. Optical absorbance was measured at 570 nm on a SpectraMax M5 microplate reader. Samples were analyzed in four independent replicates. Results are presented as % neuroprotection or half maximal effective

concentrations (EC<sub>50</sub>). Results were verified by visual inspection of the cells under a microscope.

**Intracellular Amyloid Toxicity Assay.** The assay procedure was previously described [16]. Accumulation of intracellular amyloid beta peptide (A $\beta$ ) is considered by many as being a primary toxic event in AD. The human nerve cell line MC65 conditionally expresses the C99 fragment of the amyloid precursor protein (APP) leading to the accumulation of intracellular A $\beta$ . The MC65 cells are routinely grown in the presence of tetracycline and, following its removal, the expression of C99 is induced and the cells die within three days because of the accumulation of intracellular, toxic protein aggregates. Briefly, MC65 cells were regularly grown in high glucose DMEM supplemented with 10% FCS and 2  $\mu$ g/ml tetracycline. For the assay, cells were dissociated and plated at  $1 \times 10^5$  cells per well in 24 well tissue culture plates. After overnight cultivation in growth medium, the cells were washed three times with phosphate buffered saline (PBS) containing calcium and magnesium and then switched to Opti-minimal essential media (Opti-MEM, Invitrogen) in the presence (no induction) or absence (APP-C99 induced) of 2  $\mu$ g/ml tetracycline in the presence or absence of different concentrations of the indicated compounds. At day 3, the control cells in the absence of tetracycline were mostly dead, and cell viability was determined by the MTT assay. Optical absorbance was measured at 570 nm on a SpectraMax M5 microplate reader. Samples were analyzed in three independent replicates. Results are presented as EC<sub>50</sub>s. Results were verified by visual inspection of the cells under a microscope.

**Mitochondrial Reactive Oxygen Species Measurement.** The assay procedure was previously described [12]. HT22 cells were seeded onto 96-well black walled plates at a density of 3,000 cells/well in DMEM supplemented with 10% FBS and 1% antibiotics. After the desired treatments for 16 h, mitochondrial superoxide ROS were detected with the MitoSOX Red reagent (Ex/Em = 510/580 nm). Experiments were performed according to the manufacturer's instructions. Fluorescence was measured on a SpectraMax M5 microplate reader. Data were normalized for total protein/well. Each condition was analyzed in four independent replicates. Results are presented as half maximal inhibitory concentrations (IC<sub>50</sub>). Results were verified by live-cell imaging under a fluorescence microscope.

**Lipid Peroxidation Measurements.** The assay procedures were previously described with adaptations [10,12]. HT22 cells were seeded onto 96-well black walled plates at a density of 3,000 cells/well in DMEM supplemented with 10% FBS and 1% antibiotics. After the desired treatments for 16 h, cells were labeled with 2.5  $\mu$ M C11-BODIPY 581/591 (oxidized form Ex/Em = 488/520 nm) at 37 °C for 2 h. Experiments were performed according to the manufacturer's instructions. Fluorescence was measured on a SpectraMax M5 microplate reader. Data were normalized for total protein/well. Each condition was analyzed in four independent replicates. Results are presented as half maximal inhibitory concentrations (IC<sub>50</sub>). Results were verified by live-cell imaging under a fluorescence microscope.

For the cell-free, liposome-based assay, STY-BODIPY (1.5  $\mu$ M) and liposomes of egg-PC (1 mM) in TBS (pH 7.4) were added to an opaque 96-well plate. This was followed by the addition of test compounds (5  $\mu$ M). The plate was incubated for 30 min at 37 °C and then vigorously mixed for 5 min. The autoxidation was initiated by the addition of V-70 (750  $\mu$ M) followed by additional mixing for 5 min. Data were acquired at Ex/Em = 488/518 nm every 15 min at 37 °C on a SpectraMax M5 microplate reader. Data were transformed into [ox-STY-BODIPY] by taking the raw fluorescent values of the saturated curve of the control and dividing them by the initial concentration of reduced STY-BODIPY (1.5  $\mu$ M). Samples were analyzed in four independent replicates.

**Seahorse XF Analysis.** The assay procedure was previously described [12]. Cellular oxygen consumption rates (OCR) were assayed with a XF Cell Mito Stress Test Kit, and ATP production rates were assayed with a XF Real-Time ATP Rate Assay Kit using a Seahorse XFe96 Extracellular Flux Analyzer (Agilent Technologies, Santa Clara, CA). Complete Seahorse XF DMEM assay medium was supplemented with 10

mM glucose, 1 mM pyruvate and 2 mM L-glutamine, at pH 7.4. Mitochondrial ETC inhibitors were used at the following concentrations: 1.5  $\mu$ M oligomycin, 2  $\mu$ M FCCP, and 0.5  $\mu$ M of a 1:1 mixture of rotenone and antimycin A. Analyses were conducted using Wave software and XF Report Generators (Agilent Technologies). The sensor cartridge for the XFe analyzer was hydrated overnight at 37 °C before the experiment. Data were normalized for total protein/well. Each condition was analyzed in four independent replicates. For HT22 cells, 2,000 cells/well were seeded onto the Seahorse XFe96 plates under normal culture condition as described above. The next day, cells were treated with test compounds at the desired concentrations and incubated for 16 h. Immediately before the assay, the culture medium in the plates was replaced with complete Seahorse XF DMEM assay medium. The plates were incubated for 1 h at 37 °C prior to the XF assay tests according to the manufacturer's instructions.

**Cell Protein Extraction and Quantification.** The procedure was carried out as described [17]. HT22 cells were washed with ice-cold PBS and lysed with cell extraction buffer containing 10 mM Tris, pH 7.4, 100 mM NaCl, 1 mM EDTA, 1 mM EGTA, 1 mM NaF, 20 mM Na<sub>4</sub>P<sub>2</sub>O<sub>7</sub>, 2 mM Na<sub>3</sub>VO<sub>4</sub>, 1% Triton X-100, 10% glycerol, 0.1% sodium dodecyl sulfate (SDS), 0.5% sodium deoxycholate, a protease inhibitor cocktail, and a phosphatase inhibitor cocktail followed by centrifugation (14000 g) for 30 min at 4 °C. Concentrations of the harvested proteins were determined by the BCA protein assay according to the manufacturer's instructions.

**Drosophila Stocks and Culturing Conditions.** The assay procedure has been previously described [18,19]. Briefly, adult wild-type *Drosophila melanogaster* Canton-S and *w*<sup>1118</sup> stock lines were obtained from the Bloomington *Drosophila* Stock Center. For all studies, Canton-S females were crossed with *w*<sup>1118</sup> males, to produce and maintain adult F1 outcrossed offspring (*w*<sup>1118/+</sup>) using established culturing conditions, including 25 °C, 55–65% humidity, and 12 h:12 h light:dark cycle. Male F1 flies were collected 24 h following eclosion using CO<sub>2</sub>, aged as 25 flies per vial cohorts and maintained on standard fly media (molasses, cornmeal, agar, baker's yeast) for 1 week. Cohorts were transferred to vials containing standard fly media (0.1% ethanol), or defined dosages ( $\mu$ M) of compounds (0.1% ethanol). The dosage range for the compounds was based on published *Drosophila* findings [19]. A 5 mg dose for adult flies is equivalent to about 16  $\mu$ M for the compounds or about 0.212  $\mu$ M final concentration for a whole-body human (about 75 kg) dose. Fly cohorts were maintained on food containing either CBN (3.0  $\mu$ M) or one of the analogs (3.0  $\mu$ M) for 3 weeks. To confirm palatability, flies were weighed 24 and 48 h after being placed on the compound-containing food. No significant changes in weight were observed compared with non-treated controls. As a further control, flies were placed on compound-treated food containing blue dye #1. After 4 h, 100% of flies had blue intestinal tracts.

**Drosophila Mild Traumatic Brain Injury (mTBI) Model.** TBI methods used for this study have been previously described [18,19]. Briefly, pretreated flies were anesthetized, placed in 2 mL screw cap tubes (10 flies/tube), and allowed to recover before being placed in the Omni Bead Ruptor-24 homogenizer (Omni International, Kennesaw, GA). Adult control and treated flies were pretreated for 3 days with different compounds before exposure to 10 mild trauma bouts (mild traumatic brain injury [mTBI] 10x, 2.1 m/s) at 1 week of age [19]. Following injury, flies were returned to vials containing treated media and maintained using standard culturing conditions. The number of dead flies was counted starting 48 h following trauma and then 3 times weekly for the remainder of the study, and the data were used to establish mortality indexes (MI) and longevity profiles. The percentage of dead flies described as weekly MI of treated cohorts after mTBI (10x) exposure for 1, 2 and 3 weeks was calculated. Data were normalized for total flies/cohort. Each condition includes between 110 and 235 flies (n = 110–235).

**Statistical Analysis.** Data are presented as the mean  $\pm$  SD or  $\pm$  SE as appropriate. The half maximal effective concentrations (EC<sub>50</sub>), half

maximal inhibitory concentrations ( $IC_{50}$ ), and half maximal lethal concentrations ( $LC_{50}$ ) were determined from sigmoidal dose response curves with four-parameter regression. The data were analyzed using one-way ANOVA with Tukey's multiple comparison post hoc test or Student's *t*-test as appropriate. P values for the *Drosophila* lifespan and MI were generated with the Fisher's exact test, with pairwise p-values adjusted with the Bonferroni correction. P values less than 0.05 were considered statistically significant (\* $p < 0.05$ , \*\* $p < 0.01$ , \*\*\* $p < 0.001$ , and \*\*\*\* $p < 0.0001$ ). Analyses were performed using Excel and GraphPad Prism.

### 3. Results

#### 3.1. Neuroprotective effects of fragment compounds against oxytosis/ferroptosis

As shown in Fig. 1, the structure of cannabinoids (CBN, CBD, and THC) can be divided into three substructures: a monoterpene fragment (left unit, LU), a phenol fragment (central unit, CU), and an aliphatic chain fragment (right unit, RU). To determine the most active and viable substructure(s) responsible for their neuroprotective effects, we first assayed the fragment compounds for the inhibition of oxytosis/ferroptosis using two different cytotoxic insults (i.e., glutamate and RSL3). Compounds were tested at three different concentrations (1, 10, 50  $\mu$ M) in order to cover weak to moderate bioactivities of the fragments. CBN, CBD and THC were used as reference compounds.

As summarized in Table 1, for the left unit (LU) that represents cannabinoid-relevant monoterpenoids, none of them at concentrations ranging from 1 to 50  $\mu$ M showed any neuroprotective activity in our assays. For the right unit (RU), different linear or branched aliphatic hydrocarbon chains (carbon numbers: C4–C9) were examined. As expected, these simple, water insoluble alkanes also showed no protective effects in our cell-based assays. Together, these results suggest that, by themselves, neither the LU nor the RU fragment of CBN, CBD or THC is a viable pharmacophore.

For the central unit (CU) in which the benzene ring is substituted with different numbers and positions of free hydroxyl (-OH) groups, we found that in general these simple mono- (i.e., phenol), di- (i.e., resorcinol, catechol, or hydroquinone) and tri- (i.e., phloroglucinol, pyrogallol, or hydroxyquinol) hydroxy phenols at concentrations ranging from 1 to 50  $\mu$ M showed limited neuroprotective activity against oxytosis/ferroptosis. The exceptions were the diphenols catechol (1,2-dihydroxybenzene) and hydroquinone (1,4-dihydroxybenzene) which both showed weak neuroprotective activities only at higher concentrations (10–50  $\mu$ M). Nevertheless, the data suggest that the CU fragment containing functional antioxidant groups such as aromatic hydroxyls on the phytocannabinoids are the potential key pharmacophore required for neuroprotection in our cell-based assays.

To further elaborate the crucial role of the CU in neuroprotection, we next screened combinations of substructures in our cell-based assays.

Both the LU and RU are biologically inactive in our assays. However, while the LU is structurally complex (e.g., containing cyclic structures and/or stereocenters), the RU is structurally simple (e.g., aliphatic hydrocarbon chains). Therefore, since it is challenging to readily generate a chemical library of diverse combinations of CU + LU for comprehensive analyses, combinations of CU + RU are simple and utilize commercially available alkylphenols that are more amenable for rapid chemical screening. As shown in Table 1, the monophenols substituted with linear alkyl groups (C3, C5, and C7) showed no improvement in their neuroprotective activity. The diphenols substituted with short, linear alkyl groups (from C1 to C3) showed marginal improvements in their neuroprotective activity. However, the diphenols with longer, linear alkyl chains (from C4 to C7) incrementally increased their neuroprotective activity. For example, 5-pentyl-1,3-benzenediol (olivetol), 4-hexylbenzene-1,3-diol (4-hexylresorcinol), 4-butylbenzene-1,2-diol, and 2-*tert*-butylbenzene-1,4-diol showed good to excellent neuroprotective activity at 10–50  $\mu$ M.

Biosynthetically, 5-alkylbenzene-1,3-diols (e.g., olivetol) are the precursor metabolites of the phytocannabinoids that occur naturally in the *Cannabis* plant [20,21]. We therefore took a closer look at this series of fragment compounds and their variants (Table 1). While resorcinol (benzene-1,3-diol) tends to gradually increase its neuroprotective activity as the length of its linear 5-alkyl chain is increased, the neuroprotection seems to reach an optimum when the length of the 5-alkyl chain ranges from C5 to C7. Indeed, a much longer aliphatic hydrocarbon chain like 5-pentadecylresorcinol showed no further improvement in neuroprotective activity. Similar results were also seen with the bioisosteric variants of 5-alkylbenzene-1,3-diols such as 5-butoxybenzene-1,3-diol and 5-(pentyloxy)benzene-1,3-diol where the first carbon atom on the 5-alkyl chain was replaced by an oxygen atom. However, the inclusion of a branched 5-alkyl chain such as 5-(1,1-dimethylheptyl)resorcinol greatly improved the potency of the compound (>50% neuroprotection at 1  $\mu$ M).

#### 3.2. Rational design and in silico pharmacokinetic evaluation on the new CBN analogs

Based on the resulting SAR data from the screening of the fragment compounds, we designed new CBN analogs by incorporating the CU with RU rather than LU on account of desirable bioactivity and synthetic accessibility. We selected two resorcinols, olivetol and 5-(1,1-dimethylheptyl)resorcinol, as the candidate building blocks for the CU + RU. In addition, a portion of the LU of CBN was removed with the goal of decreasing the molecular weight and lipophilicity of the CBN analogs because these two molecular properties are the most important factors in influencing the pharmacokinetics and pharmacodynamics of drug candidates [22–24]. Instead, a simplified version of the benzopyran ring system as the LU was designed in order to retain the structural rigidity and relevant bioactivity [25,26]. Following our previously reported protocol with modifications [12], combinatorial chemistry was then

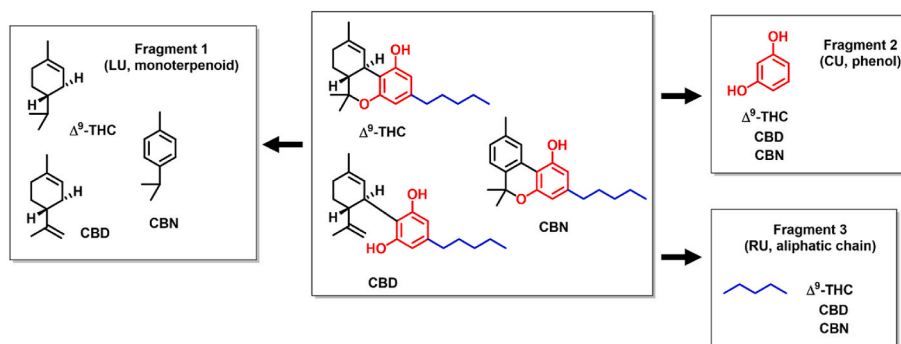
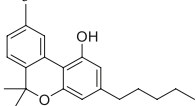
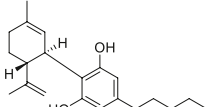
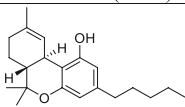
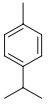
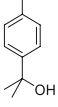
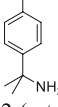
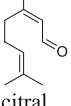
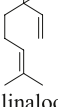
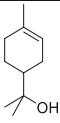
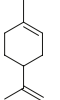
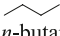
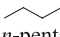
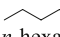
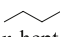
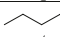
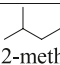
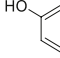
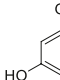
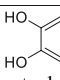
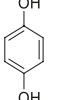
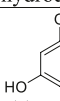
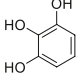
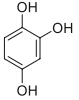
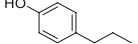
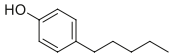
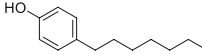
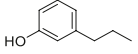
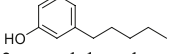
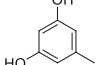
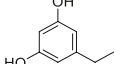
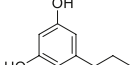
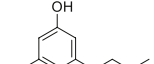
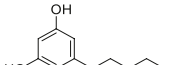


Fig. 1. Structural analyses of cannabinoids using a fragment-based drug discovery (FBDD) approach.

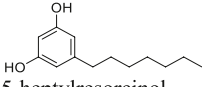
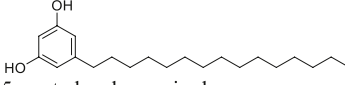
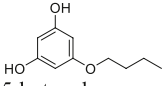
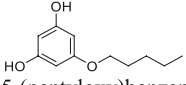
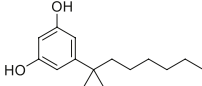
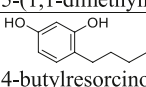
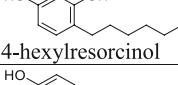
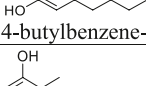
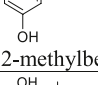
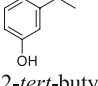
**Table 1**  
Neuroprotective activities of compound fragments against inducers of oxytosis/ferroptosis.

Compound	Oxytosis Glutamate (5 mM)			Ferroptosis RSL3 (100 nM)		
	50 $\mu$ M	10 $\mu$ M	1 $\mu$ M	50 $\mu$ M	10 $\mu$ M	1 $\mu$ M
<b>Reference cannabinoids</b>						
 cannabiniol (CBN)	++++	+++	++	++++	+++	++
 cannabidiol (CBD)	++++	+++	++	++++	+++	++
 tetrahydrocannabinol (THC)	++++	+++	++	++++	+++	++
<b>Left unit (LU)</b>						
 p-cymene	-	-	-	-	-	-
 p,α,α-trimethylbenzyl alcohol	-	-	-	-	-	-
 2-(p-tolyl)propan-2-amine	-	-	-	-	-	-
 citral	-	-	-	-	-	-
 linalool	-	-	-	-	-	-

	-	-	-	-	-	-	-
$\alpha$ -terpineol							
	-	-	-	-	-	-	-
limonene							
<b>Right unit (RU)</b>							
	-	-	-	-	-	-	-
<i>n</i> -butane							
	-	-	-	-	-	-	-
<i>n</i> -pentane							
	-	-	-	-	-	-	-
<i>n</i> -hexane							
	-	-	-	-	-	-	-
<i>n</i> -heptane							
	-	-	-	-	-	-	-
<i>n</i> -octane							
	-	-	-	-	-	-	-
2-methyloctane							
<b>Central unit (CU)</b>							
	-	-	-	-	-	-	-
phenol							
	-	-	-	-	-	-	-
resorcinol							
	++	+	-	++	+	-	-
catechol							
	-	-	-	++	+	-	-
hydroquinone							
	-	-	-	-	-	-	-
phloroglucinol							

	-	-	-	-	-	-
pyrogallol	-	-	-	-	-	-
	-	-	-	-	-	-
hydroxyquinol	-	-	-	-	-	-
<b>CU+RU (Mono-phenols)</b>						
	-	-	-	-	-	-
4-propylphenol	-	-	-	-	-	-
	-	-	-	-	-	-
4-pentylphenol	-	-	-	-	-	-
	-	-	-	-	-	-
4-heptylphenol	-	-	-	-	-	-
	-	-	-	-	-	-
3-propylphenol	-	-	-	-	-	-
	-	-	-	-	-	-
3-pentylphenol	-	-	-	-	-	-
<b>CU+RU (Di-phenols)</b>						
	-	-	-	-	-	-
5-methylresorcinol	-	-	-	-	-	-
	-	-	-	+	-	-
5-ethyl-1,3-benzenediol	-	-	-	+	-	-
	+	-	-	+	-	-
5-propylbenzene-1,3-diol	+	-	-	+	-	-
	+	-	-	+	-	-
5-butylresorcinol	+	-	-	+	-	-
	++	+	-	++	+	-
5-pentyl-1,3-benzenediol (olivetol)	++	+	-	++	+	-



 5-heptylresorcinol	++	+	-	++	+	-
 5-pentadecylresorcinol	++	+	-	++	+	-
 5-butoxybenzene-1,3-diol	++	+	-	++	+	-
 5-(pentylloxy)benzene-1,3-diol	++	+	-	++	+	-
 5-(1,1-dimethylheptyl)resorcinol	+++	++	+	+++	++	+
 4-butylresorcinol	+	-	-	+	-	-
 4-hexylresorcinol	++	+	-	++	+	-
 4-butylbenzene-1,2-diol	++	+	-	+++	++	+
 2-methylbenzene-1,4-diol	-	-	-	++	+	-
 2-tert-butylbenzene-1,4-diol	++	+	-	++	+	-

Heatmap and symbol representation of % neuroprotection: - (<50%), + (50–60%), ++ (60–75%), +++ (75–85%), ++++ (85–100%).

performed (Fig. 2). A one-step total synthesis through amine-catalyzed reactions of resorcinols with  $\alpha,\beta$ -unsaturated aldehydes (i.e., senecialdehyde and crotonaldehyde) resulted in the production of four new CBN analogs (CP1 to CP4) in high yields.

CBN and the new analogs were initially subjected to *in silico* pharmacokinetic evaluation using the SwissADME tool [14]. As shown in Table 2, in general, the new analogs have a smaller molecular weight (MW) and lower lipophilicity (MLogP) relative to CBN. They also show an improvement in water solubility compared to CBN. Most importantly, the four new analogs were predicted to be blood-brain barrier (BBB) permeable, which is critical for CNS drug development [27].

### 3.3. Neuroprotective effects of the new CBN analogs against oxytosis/ferroptosis

Next, we screened the new analogs (CP1 to CP4) along with CBN as a reference control in the oxytosis/ferroptosis assays to determine their neuroprotective activities against three distinct insults: RSL3 (50 nM), glutamate (5 mM), and erastin (500 nM) at subtoxic concentrations (based on LC<sub>50</sub> values of the insults, see Supplementary Fig. S6). As shown in Table 3, the new analogs CP1-CP4 have strong neuroprotective effects against RSL3-induced oxytosis/ferroptosis with EC<sub>50</sub> values ranging from 0.68 to 0.92  $\mu$ M. These potencies are comparable to that of

CBN (EC<sub>50</sub>, 0.69  $\mu$ M). Similar neuroprotective effects of the new analogs were also seen against glutamate- or erastin-induced oxytosis/ferroptosis, although their EC<sub>50</sub> values of low micromolar levels are somewhat higher than those for protection against RSL3 toxicity. Interestingly, among the four analogs, CP1 showed the strongest potencies against the three insults and its EC<sub>50</sub> values are comparable to those of CBN.

### 3.4. Neuroprotective effects of the new CBN analogs against intracellular amyloid toxicity

We previously reported that intracellular amyloid toxicity shares many pathophysiological characteristics with the oxytosis/ferroptosis regulated cell death pathway and CBN is highly protective against intracellular amyloid toxicity [11,16]. Thus, we investigated whether the new analogs possess similar protective profiles against intracellular amyloid toxicity in MC65 cells as compared to CBN.

As shown in Table 3, the new analogs showed sub-micromolar potencies against intracellular amyloid toxicity (EC<sub>50</sub>s from 31 to 1600 nM) as compared with CBN (EC<sub>50</sub>, 14 nM). Consistent with the data from the other screens, CP1 (EC<sub>50</sub>, 31 nM) was the most potent analog in this assay.

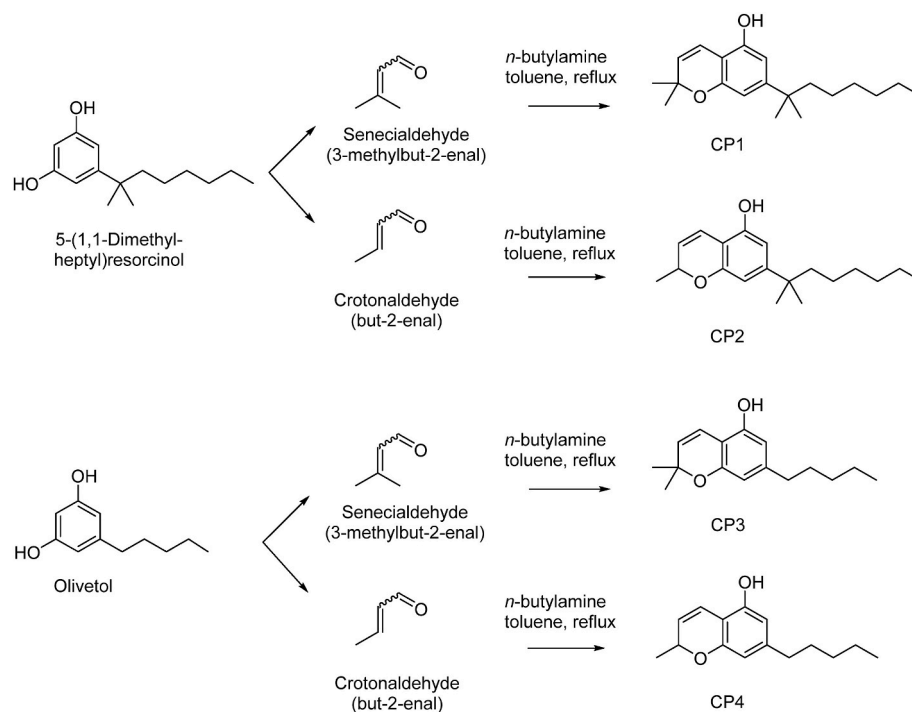


Fig. 2. Scheme for the total synthesis of CP1-CP4.

Table 2

Predicted physicochemical properties of CBN and the new analogs.

Compound	MW	MLogP	TPSA ( $\text{\AA}^2$ )	HBDS (n.OH,NH)	HBAs (n.O,N)	Water solubility	BBB permeant
Desired CNS druglikeness	$\leq 360$	$\leq 4.15$	$\leq 90$	$\leq 3$	$\leq 7$	soluble	yes
CBN	310	4.23	29.46	1	2	poor	yes
CP1	302	4.17	29.46	1	2	moderate	yes
CP2	288	3.94	29.46	1	2	moderate	yes
CP3	246	3.23	29.46	1	2	moderate	yes
CP4	232	2.98	29.46	1	2	moderate	yes

Desired CNS druglikeness should present as molecular weight (MW)  $\leq 360$ , calculated partition coefficient (MLogP)  $\leq 4.15$ , topological polar surface area (TPSA)  $\leq 90$ , number of hydrogen-bond donors (HBDS)  $\leq 3$ , and number of hydrogen-bond acceptors (HBAs)  $\leq 7$  to improve penetration of the blood-brain barrier (BBB). Predictions were calculated with the SwissADME tool. For additional information see Supplementary Figures S1–S5.

Table 3

Neuroprotective activities of CBN and the new analogs.

Compound	RSL3 (EC <sub>50</sub> , $\mu\text{M}$ )	Glutamate (EC <sub>50</sub> , $\mu\text{M}$ )	Erastin (EC <sub>50</sub> , $\mu\text{M}$ )	A $\beta$ toxicity (EC <sub>50</sub> , nM)
CBN	0.69	1.9	2.3	14
CP1	0.68	1.9	2.8	31
CP2	0.92	2.9	3.4	97
CP3	0.86	2.6	3.8	144
CP4	0.83	6.6	8.1	1600

For all of the insults tested, the EC<sub>50</sub>s for protection by each of the compounds are indicated in the columns. RSL3 (50 nM), glutamate (5 mM), and erastin (500 nM) were used as oxytotic/ferroptotic insults in the HT22 cells. The A $\beta$  protection assay used MC65 cells.

### 3.5. Antioxidant effects of the new CBN analogs against oxytosis/ferroptosis

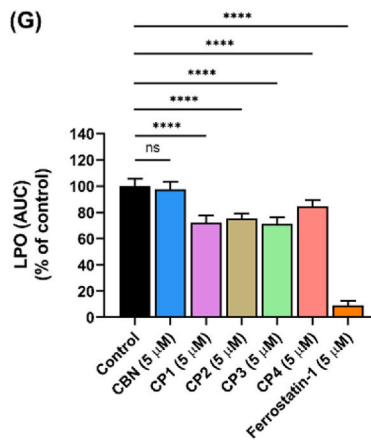
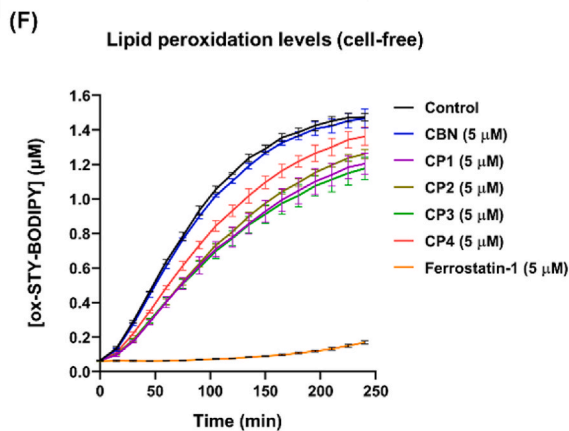
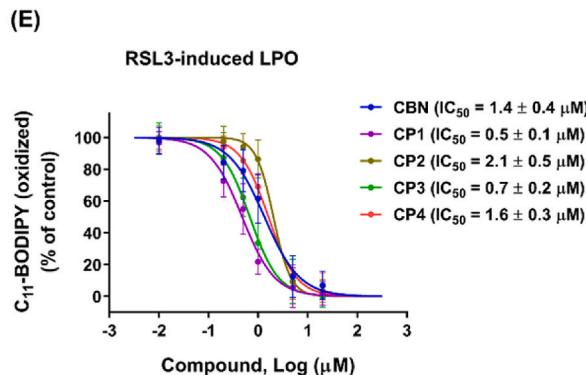
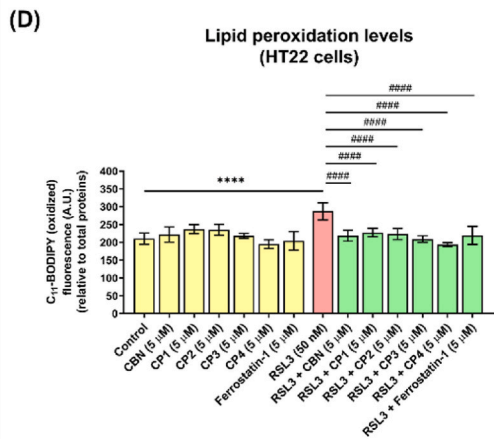
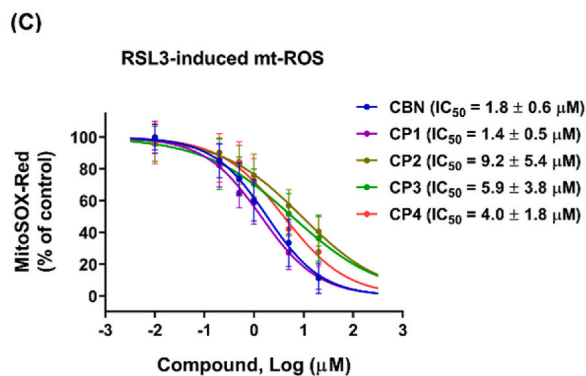
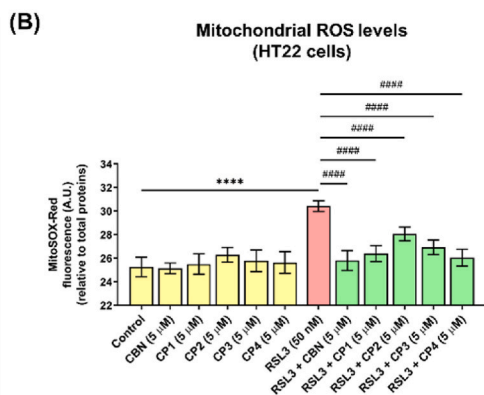
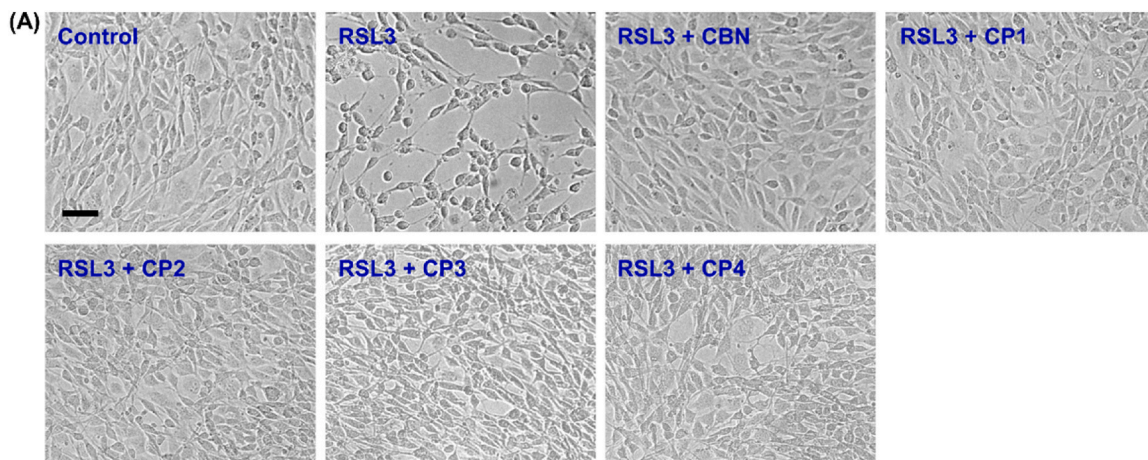
Activation of the oxytosis/ferroptosis pathway causes an elevation in cellular oxidative stress, particularly in mitochondria, where mitochondrial ROS (mtROS) contribute to the lipid peroxidation (LPO) of cellular membranes [9,28,29]. We previously found that CBN is an indirect antioxidant that activates endogenous antioxidant defenses resulting in the maintenance of cellular morphology and strong

inhibition against the cascade of mitochondrial oxidative stress caused by induction of oxytosis/ferroptosis [12]. Hence, we next tested the antioxidant parameters (i.e., anti-mtROS and anti-LPO) of the four new analogs in comparison with CBN in HT22 cells treated with RSL3.

As shown in Fig. 3A, microscopic imaging clearly showed that treatment with RSL3 (50 nM) led to dramatic changes in cellular morphology with large numbers of rounded and shrinking cells present as compared to the control group. Cotreatment of RSL3 with 5  $\mu\text{M}$  CBN or the individual analogs effectively prevented these morphological alterations in HT22 cells.

Further evaluation of the levels of oxidative stress (Fig. 3B) indicated that the four analogs of CBN at 5  $\mu\text{M}$  alone did not affect the redox status of mitochondria following treatment in HT22 cells. However, the cells treated with 50 nM RSL3 showed a significant increase in mtROS in comparison to the control cells ( $p < 0.0001$ ). Treatment with either CBN or the different analogs at 5  $\mu\text{M}$  significantly suppressed RSL3-induced mtROS production. Quantitative dose-response measurements for the four analogs along with CBN (Fig. 3C) indicated that CP1 (IC<sub>50</sub>, 1.4  $\mu\text{M}$ ) showed the strongest anti-mtROS effect, similar to that of CBN (IC<sub>50</sub>, 1.8  $\mu\text{M}$ ), whereas the other three analogs had higher IC<sub>50</sub> values ranging from 4.0 to 9.2  $\mu\text{M}$ .

Regarding lipid peroxidation (LPO), the compounds (CBN and CP1-CP4) alone tested at 5  $\mu\text{M}$  did not change the LPO levels in control HT22 cells (Fig. 3D). However, treatment with the analogs or CBN



(caption on next page)

**Fig. 3.** Antioxidant effects of the new CBN analogs against oxytosis/ferroptosis in HT22 cells. (A) Representative micrographs of HT22 cells following different treatments for 16 h: vehicle control, 50 nM RSL3, 50 nM RSL3 + 5  $\mu$ M CBN, 50 nM RSL3 + 5  $\mu$ M CP1, 50 nM RSL3 + 5  $\mu$ M CP2, 50 nM RSL3 + 5  $\mu$ M CP3, 50 nM RSL3 + 5  $\mu$ M CP4. Micrographs show the representative morphological characteristics of the cell cultures under a given condition of eight independent replicates. Scale bar = 200  $\mu$ m. (B) Mitochondrial ROS levels following different treatments of the cells for 16 h. Data were normalized to total protein/well and are the mean of four independent replicates per condition  $\pm$  SD. (C) Dose-response inhibitory curves and IC<sub>50</sub> values of the compounds against RSL3-induced mitoROS. 50 nM of RSL3 treated in cells. Data are the mean of four independent replicates per condition  $\pm$  SD. (D) Cellular lipid peroxidation levels following different treatments of the cells for 16 h. Data were normalized to total protein/well and are the mean of four independent replicates per condition  $\pm$  SD. (E) Dose-response inhibitory curves and IC<sub>50</sub> values of the compounds against RSL3-induced LPO. 50 nM of RSL3 treated in cells. Data are the mean of four independent replicates per condition  $\pm$  SD. (F) Time course of lipid peroxidation levels following different treatment conditions in a cell-free system. 5  $\mu$ M of compounds tested. Data are the mean of four independent replicates per condition  $\pm$  SD. (G) Quantitative analysis of the cell-free LPO levels (area under the curve). Data are the mean of four independent replicates per condition  $\pm$  SD. All data were analyzed by one-way ANOVA with Tukey's multiple comparison test. \*\*\*\*p < 0.0001 relative to vehicle control; #####p < 0.0001 relative to the 50 nM RSL3 treatment; ns, not significant.

significantly suppressed the RSL3-induced increase in intracellular LPO ( $p < 0.0001$ ), which was similar to the effect of ferrostatin-1 (5  $\mu$ M), a known LPO and oxytosis/ferroptosis inhibitor used as a reference control in our study. Quantitative dose-response measurements of cellular LPO levels (Fig. 3E) for the compounds indicated that CP1 (IC<sub>50</sub>, 0.5  $\mu$ M) and CP3 (IC<sub>50</sub>, 0.7  $\mu$ M) are more potent than CBN (IC<sub>50</sub>, 1.4  $\mu$ M) at preventing RSL3-induced lipid peroxidation, while CP2 (IC<sub>50</sub>, 2.1  $\mu$ M) and CP4 (IC<sub>50</sub>, 1.6  $\mu$ M) are relatively less potent than CBN.

To examine if the antioxidant effects of the analogs in cells are due to their inherent anti-oxidation activities [30], the compounds at 5  $\mu$ M were further tested in a cell-free, liposome-based assay of lipid peroxidation (Fig. 3F and G). Interestingly, unlike CBN that has no direct inhibition against lipid autoxidation by trapping peroxy radicals, CP1-CP4 have moderate activities as radical-trapping antioxidants (RTAs) (ranging from 15 to 30% suppression of LPO relative to the control). Among them, CP1 (72% of LPO) and CP3 (71% of LPO) showed slightly better inhibitory effects than CP2 (75% of LPO) and CP4 (85% of LPO). Conversely, the reference RTA, ferrostatin-1 (5  $\mu$ M), showed a very potent, direct effect against lipid peroxidation (9% of LPO) in the cell-free assay.

Together, the results demonstrate that like CBN, the new analogs are very cytoprotective and effective at preventing increases in mtROS and LPO in cells induced by an activator of oxytosis/ferroptosis. Additionally, distinct from CBN, the analogs exert direct but moderate anti-oxidative action. Furthermore, in these assays looking at both indirect and direct inhibition of lipid peroxidation, CP1 stood out as being superior to CBN.

### 3.6. Mitochondrial modulatory effects of the new CBN analogs against oxytosis/ferroptosis

Previously, we reported that CBN targets mitochondria and modulates their function including mitochondrial bioenergetics in cells and that this effect of CBN is independent of canonical CB1/CB2 receptor signalling [12]. Thus, we wanted to determine if the new CBN analogs would also possess similar mitochondrial modulatory effects. Therefore, CBN and CP1-CP4 along with the oxytotic/ferroptotic inducer RSL3 were assayed in the Seahorse XF real-time ATP rate and mitochondrial stress assays, which can be used to evaluate the phenotypic changes in mitochondrial metabolism upon compound treatment in cells.

In cells, ATP production is known to involve both mitochondrial oxidative phosphorylation (OXPHOS) and cytosolic glycolysis. The Seahorse ATP rate assay can be used to study the cellular dependency of metabolic phenotypes for ATP production as well as to characterize compounds inducing metabolic switches [31–34]. As shown in Fig. 4A, in HT22 neuronal cells the four analogs and CBN at 5  $\mu$ M slightly but significantly decreased total ATP production rate to a similar level as compared to the control (about 20–28% decrease). In contrast, RSL3 at 50 nM caused a substantial decrease in total ATP production rate (68% decrease). CBN and the four analogs appear to have a much greater impact on reducing the rates of glyco-ATP production (40–51% decrease) as compared with mito-ATP production (5–20% decrease) (Fig. 4B and C), which led to the partial decrease in the total ATP

production rate in the HT22 cells. RSL3 treatment, however, significantly reduced both the mito-ATP and glyco-ATP production rates at 79% and 53%, respectively.

With regard to the percent contribution of mito-ATP and glyco-ATP production rates to the total ATP production rate (Fig. 4D) and as represented by the ATP rate index (a ratio of mito-ATP/glyco-ATP) (Fig. 4E), the mito-ATP production rate in the control HT22 cells contributed about 59% to the total ATP production rate while in the CBN and the analog-treated cells, the mito-ATP production rate contributed 10–15% more to the total ATP production rate (69–74%). An increase in the ATP rate index by CBN and the analogs ( $p < 0.0001$ ) (Fig. 4E) also suggested that they stimulated the cells to rely on a more mitochondrial and less glycolytic metabolic phenotype, potentially driving their neuroprotective functions. In contrast, RSL3-treated cells switched the energy phenotype to become more glycolytic (60%) than OXPHOS-dependent (40%) with concomitant impaired total ATP production.

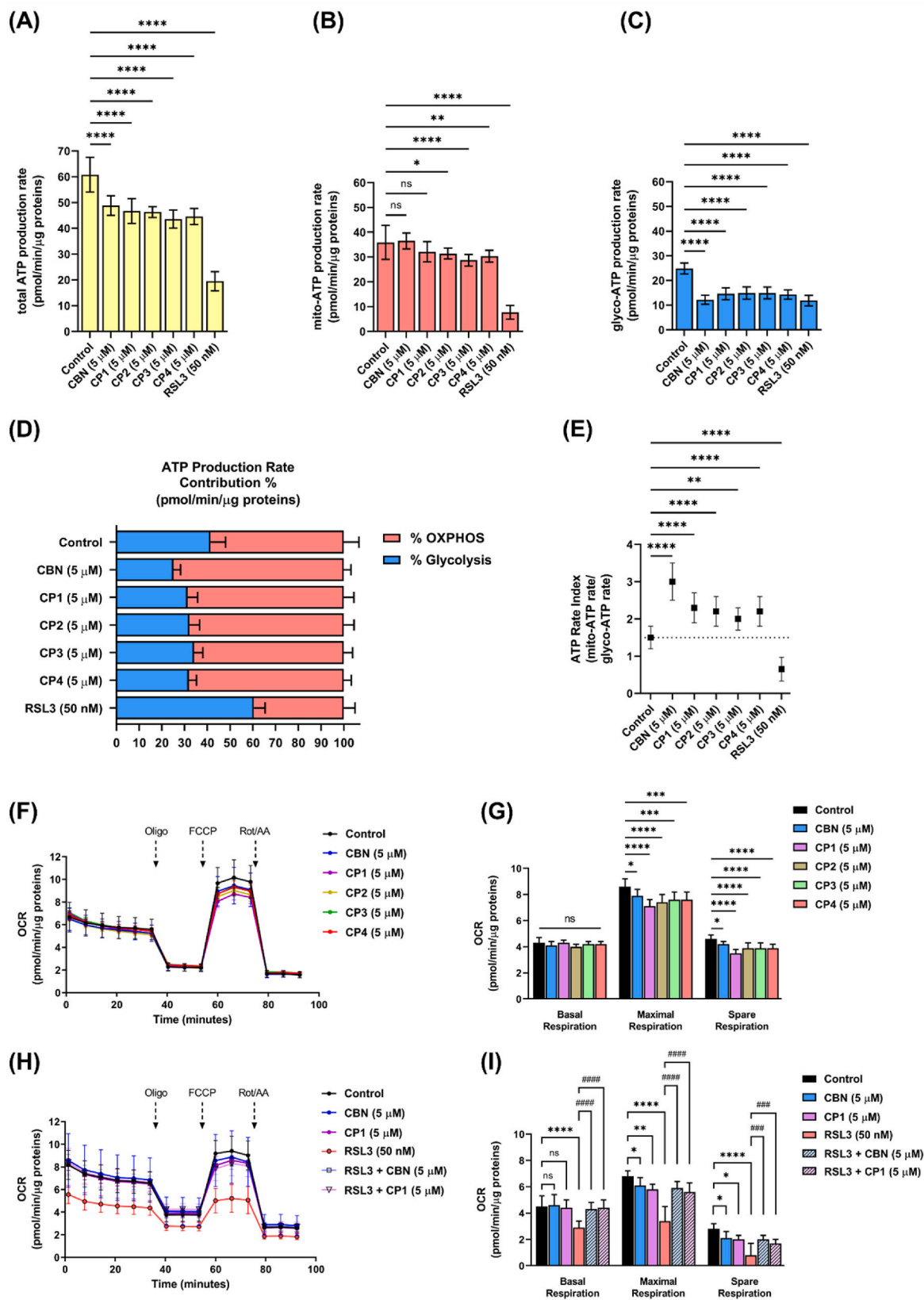
For the mitochondrial stress test (Fig. 4F and G), HT22 cells treated with CBN or the individual analogs showed a small but significant decrease in maximal and spare mitochondrial respiration as compared with the control cells. Among them, CP1 showed the strongest effect on the suppression of maximal/spare OCR. In contrast, the basal respiration was not significantly affected by the compounds. To correlate the mitochondrial modulatory effects to the neuroprotection against oxytosis/ferroptosis, CBN and the best analog, CP1, were further assayed in HT22 cells under RSL3 exposure. Pairwise comparisons (Fig. 4H and I) illustrated that RSL3 at 50 nM markedly depressed basal, maximal, and spare mitochondrial respiration. However, HT22 cells treated with 5  $\mu$ M of CBN or CP1 followed by RSL3 treatment for 16 h showed a maintenance of mitochondrial respiration at levels similar to the compound-treatment alone.

Taken together, the Seahorse assay findings indicate that the CBN analogs have a similar mechanism of action on mitochondria as the parent compound CBN, modulating mitochondrial function and bioenergetic phenotype for neuroprotection within cells.

### 3.7. In vivo efficacy of the new CBN analogs in the *Drosophila* mild traumatic brain injury (mTBI) model

Traumatic brain injury (TBI) is a complicated form of neurological disorder, and its pathological processes involve complex fluctuations of inflammation and mitochondrial dysfunction in brain cells [18,35]. Emerging evidence indicates that TBI is also a risk factor for AD and other neurodegenerative diseases [36]. Moreover, recent research reveals that the negative outcomes after TBI are potentially linked to activation of the oxytosis/ferroptosis cell death pathway [37,38]. Thus, we used the *Drosophila* mTBI model to test our analogs in parallel with CBN and evaluate their *in vivo* neuroprotective efficacy.

As shown in Fig. 5A–C, relative to the control fly cohort (an average lifespan of 27.3 days), treatment of flies with 3  $\mu$ M of CBN or the analogs following mTBI (10x) exposure showed a significant, positive impact of CBN and CP1 on the promotion of overall longevity of 2.5 days (9.4%,  $p = 0.010$ ) and 3.2 days (11.9%,  $p = 0.0018$ ), respectively. While not significant, a modest impact on longevity was also observed for CP2



(caption on next page)

**Fig. 4.** Mitochondrial modulatory effects of the new CBN analogs. (A) Total ATP production rate, (B) mito-ATP production rate, and (C) glyco-ATP production rate in HT22 cells after the different treatments for 16 h. 5  $\mu\text{M}$  of compounds or 50 nM of RSL3 treated in cells. Data were normalized to total protein/well and are the mean of four independent replicates per condition  $\pm$  SD. (D) Relative contribution of ATP production from oxidative phosphorylation (OXPHOS) and glycolysis to total ATP production in HT22 cells. Data are the mean of four independent replicates per condition  $\pm$  SD. (E) ATP rate index. Dotted line depicts the control level. Data are the mean of four independent replicates per condition  $\pm$  SD. (F) Mitochondrial oxygen consumption rate (OCR) profiles in HT22 cells in control and compound treated cells at 16 h. 5  $\mu\text{M}$  of compounds or 50 nM of RSL3 treated in cells. Data were normalized to total protein/well and are the mean of four independent replicates per condition  $\pm$  SD. (G) Graph showing basal respiration, maximal respiration, and spare respiration in control and compound treated HT22 cells. Data are the mean of four independent replicates per condition  $\pm$  SD. (H) Mitochondrial oxygen consumption rate (OCR) profiles in HT22 cells in control and compound treated cells after RSL3 exposure at 16 h. 5  $\mu\text{M}$  of compounds or 50 nM of RSL3 treated in cells. Data were normalized to total protein/well and are the mean of four independent replicates per condition  $\pm$  SD. (I) Graph showing basal respiration, maximal respiration, and spare respiration in control and compound treated HT22 cells. Data are the mean of four independent replicates per condition  $\pm$  SD. All data were analyzed by one-way ANOVA with Tukey's multiple comparison test. \* $p < 0.05$ , \*\* $p < 0.01$ , \*\*\* $p < 0.001$ , \*\*\*\* $p < 0.0001$  relative to vehicle control; ### $p < 0.001$ , #### $p < 0.0001$  relative to the 50 nM RSL3 treatment; ns, not significant.

(4.3%), CP3 (2.3%) and CP4 (1.1%) treated cohorts (3  $\mu\text{M}$  dosage). The weekly death counts (Fig. 5D) also revealed a positive trend in that CBN and the analogs helped to decrease the fly mortality although the effects were not initially significant in the first two weeks. By 3 weeks post-mTBI, approximately 70% of the vehicle-treated control flies were dead ( $\text{MI}^{-3\text{week}}$ ). In contrast, all of the treatment cohorts showed a

decrease in mortality that ranged from 49.5 to 67.3%  $\text{MI}^{-3\text{week}}$ . This decrease was significant for the CP1-treated cohort where the  $\text{MI}^{-3\text{week}}$  went from 70.2% to 49.5% ( $p = 0.0043$ ). The protective effects of CBN ( $\text{MI}^{-3\text{week}}$ , 60.5%) and CP4 ( $\text{MI}^{-3\text{week}}$ , 61.9%) treatments against mTBI-induced mortality were also notable, although not statistically significant, while CP2 ( $\text{MI}^{-3\text{week}}$ , 66.7%) and CP3 ( $\text{MI}^{-3\text{week}}$ , 67.3%)

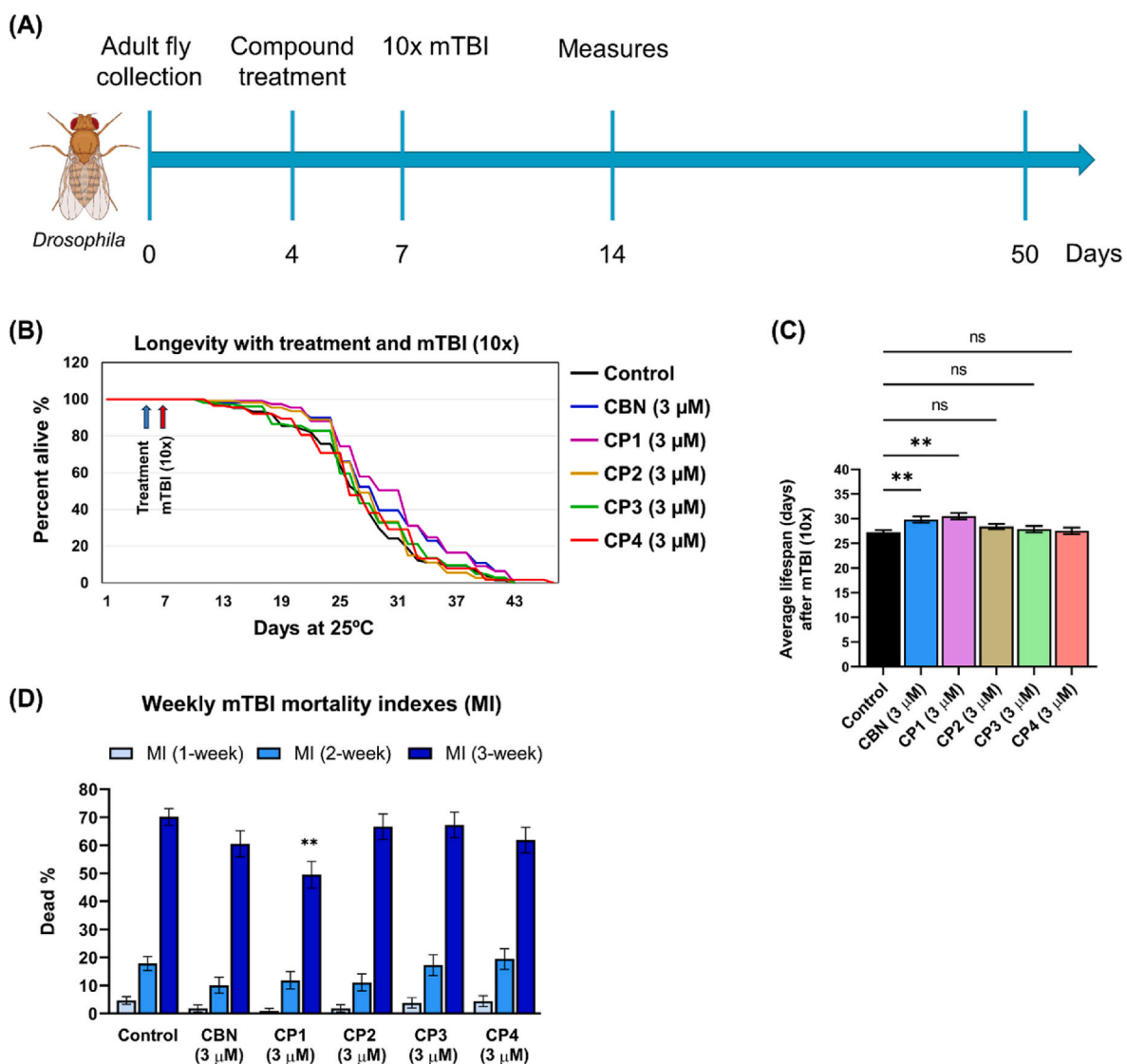


**Fig. 5.** Longevity and mortality profiles of CBN and analog-treated flies following mTBI (10x) exposure. (A) Treatment and mTBI study timeline. (B) Kaplan-Meier survival profiles for each fly cohort following mTBI exposure. (C) Average lifespan profiles for each fly cohort. 3  $\mu\text{M}$  of compounds treated in flies. Data are the mean of 110–235 flies per condition  $\pm$  SE. (D) The percentage of dead flies or mortality index (MI) was calculated for the different fly cohorts at 1 week, 2 weeks, and 3 weeks following mTBI (10x) exposure. 3  $\mu\text{M}$  of compounds treated in flies. Data were normalized to total flies/cohort and are the mean of 110–235 flies per condition  $\pm$  SE. For additional information see [Supplementary Tables S1–2](#). Value comparisons were analyzed using one-way ANOVA with Tukey's multiple comparison test. \*\* $p < 0.01$  relative to vehicle control; ns, not significant.

treatments had marginal, positive effects on *in vivo* trauma responses. Overall, the *Drosophila* mTBI studies demonstrate the *in vivo* beneficial effects of the new analogs, where not only was CP1 the best of the analogs but was also more efficacious than the parent compound, CBN.

#### 4. Discussion

Oxytosis/ferroptosis is a novel form of regulated cell death that has gained increasing attention due to its possible involvement in many neurological disorders [8,9,39]. In our continued efforts to identify natural product-based inhibitors of oxytosis/ferroptosis [11,15,40,41], we recently screened a large number of natural and synthetic cannabinoids using our cell-based phenotypic assays [11] and found that the non-psychoactive phytocannabinoid, cannabidiol (CBD), is highly neuroprotective [11,12]. CBN showed sub-low micromolar potency ( $EC_{50}$ ) against different inducers of oxytosis/ferroptosis and it appeared to do so by modulating multiple aspects of mitochondrial function [12]. In addition, CBN has positive CNS druglike properties (MW = 310, MLogP = 4.23, PSA = 29.46, HBD = 1, HBA = 2) along with good safety and pharmacokinetic profiles in humans [42–44]. These findings indicate that CBN has promise as a drug lead for the treatment of neurological disorders. However, from a medicinal chemistry point of view, there remain multiple questions pertaining to the structural requirements and chemical space of CBN necessary for the inhibition of oxytosis/ferroptosis. This information is critical for the rational design of new CBN analogs with improved potency and CNS druglikeness [23].

In the present study, we used a fragment-based method to systematically analyze the SAR of CBN [13]. For this analysis, the structure of CBN was divided into three basic fragment units: a monoterpenoid fragment (left unit, LU), a phenol fragment (central unit, CU), and an aliphatic chain fragment (right unit, RU) (Fig. 1). A series of fragments with different variants of the basic substructures were first screened in our cell-based phenotypic assays for protection against oxytosis/ferroptosis. Our results (Table 1) clearly showed that neither the LU nor the RU alone is a bioactive pharmacophore of CBN. In contrast, the CU with functional antioxidant groups such as aromatic hydroxyls showed modest neuroprotection in a dose-dependent manner in our biological assays. Moreover, by attaching a RU to the CU we were able to significantly increase the potency of this fragment against oxytosis/ferroptosis. Thus, the overall SAR analysis indicated that the CU is a critical pharmacophoric element of CBN. Because the RU is a lipophilic, long-chain hydrocarbon, its addition to a CU likely facilitates the improvement of compound potency by incrementally increasing cell membrane permeability and improving the physiochemical properties of the compound. However, the SAR study was limited owing to the synthetic accessibility for combinations of LU and CU, and it is possible that the LU due to its lipophilic, cyclic nature could also modulate the potency of the compounds. The contribution of the LU to SAR deserves further study.

Based on the SAR information on CBN from the FBDD method, we therefore designed and synthesized four new analogs, CP1 to CP4 (Fig. 2). The structure of the newly designed analogs contains the CU + RU derived from either olivetol or 5-(1,1-dimethylheptyl)resorcinol, the two best 5-alkylbenzene-1,3-diols identified in the screening of fragment compounds (Table 1). In addition, a simplified version of the benzopyran ring system was included as the LU in order to retain the structural rigidity and relevant bioactivity of CBN [25,26]. *In silico* pharmacokinetic evaluation with the SwissADME tool suggested that these four analogs generally possess better CNS druglike properties than CBN in terms of smaller molecular weights, a better balance of lipophilicity/hydrophilicity and BBB permeability (Table 2). The four CBN analogs also showed strong neuroprotection in our cell-based models against RSL3-, glutamate-, erastin- and  $\beta$ -induced oxytosis/ferroptosis (Table 3). Among them, CP1 is the best with  $EC_{50}$  values ranging from 31 nM to 2.8  $\mu$ M in the different neuroprotection assays. These potencies are comparable to those of the parent compound CBN. These analogs,

particularly CP1, also effectively prevented changes in cellular morphology and suppressed markers of cellular oxidative stress (i.e., mtROS and LPO) seen following induction of oxytosis/ferroptosis (Fig. 3). Importantly, CP1 ( $IC_{50}$ , 0.5  $\mu$ M) is more potent than CBN ( $IC_{50}$ , 1.4  $\mu$ M) against cellular LPO. Furthermore, distinct from CBN, the four analogs are moderate radical-trapping antioxidants (RTAs) although their activities are much lower than ferostatin-1, a known RTA, which was tested at the same concentration in the cell-free assay for inhibition of LPO. Collectively, the data suggest that the new analogs might have synergistic mechanisms by which they both indirectly and directly inhibit RSL3-induced lipid peroxidation, potentially expanding their overall anti-oxytotic/ferroptotic effects.

Notably, the superior potencies of CP1 to the other three analogs are plausibly due to the subtle but critical differences in their chemical structures (Fig. 2 and Table 3). Although all four analogs are structurally similar, CP1 contains a 2,2-dimethyl-2H-pyran group and a 1,1-dimethylheptyl group on its LU and RU, respectively. These two branched dimethyl groups could serve as molecular anchors into cytoplasmic/mitochondrial membranes, thereby potentially improving its target engagement for neuroprotection against oxytosis/ferroptosis. In contrast, CP2 with a 2-methyl-2H-pyran group on the LU appears to have a slightly decreased potency. On the other hand, while CP3 retains a 2,2-dimethyl-2H-pyran group on the LU, replacement with a linear pentyl group on the RU of CP3 also results in a small decrease in potency relative to CP1. Consistent with these observations, CP4, without either branched dimethyl group, is the least potent analog.

Previously we showed that the neuroprotective effects of CBN against oxytosis/ferroptosis were dependent on the modulation of mitochondrial function. We found that all four CBN analogs also appeared to modulate mitochondria and their metabolic phenotypes in cells (Fig. 4). Similar to CBN, they slightly dampened mitochondrial oxygen consumption (i.e., maximal/spare OCR and total ATP production rate) but proportionally enhanced the mitochondrial OXPHOS dependency for ATP production. On the contrary, the oxytotic/ferroptotic inducer, RSL3, substantially diminished mitochondrial oxygen consumption and switched the cells to be primarily glycolytic. This shift in ATP generation between OXPHOS and glycolysis as well as the restorative effect of mitochondrial respiration against RSL3 upon treatment with CBN and the new analogs further supports a potential mode of action in terms of mitochondrial modulation and cellular bioenergetics [32–34]. By correlating with their antioxidant effects (Fig. 3), it is conceivable that these analogs partially reduce mitochondrial respiration and at the same time suppress aberrant mitochondrial ROS production which consequently protect cells from ROS-mediated toxic lipid peroxidation and oxytosis/ferroptosis. Our results highlight the role of mitochondrial OXPHOS as an energy supplier for cell protection.

Traumatic brain injury (TBI) reflects an acute form of brain dysfunction caused by external forces to the head. In multiple models, TBI leads to elevated oxidative stress, lipid peroxidation, autophagic/lysosomal and mitochondrial dysfunction in brain cells as well as increased levels of inflammation, with downstream effects including the loss of axonal connections and eventually nerve cell death [35,45]. Epidemiological studies have consistently linked head trauma to a greater risk for AD and related dementias [36,46]. Interestingly, current evidence suggests a possible role for oxytosis/ferroptosis in TBI pathology and there is growing evidence that inhibition of oxytosis/ferroptosis can help to alleviate the long-term outcomes of TBI [38,39].

*Drosophila melanogaster* (fruit flies) have emerged as an excellent model organism for studying the mechanisms underpinning a range of neurodegenerative and neurological disorders [47,48]. As non-mammalian models, they have some limitations as well as enormous values in early biomedical research [49,50]. We recently reported that using our *Drosophila* model of mild traumatic brain injury (mTBI), phytocannabinoids, including cannabidiol (CBD) and  $\Delta^9$ -tetrahydrocannabinol (THC), were also neuroprotective [18,19]. Together, the

*Drosophila* mTBI model can serve as a rapid, inexpensive, and highly effective tool to screen and evaluate the *in vivo* therapeutic potential of additional, cannabinoid-based compounds under conditions of acute and protracted neural stress. Here, we assayed CBN and its analogs using the *Drosophila* mTBI model to further assess their *in vivo* pharmacological efficacy. Over the entirety of 50-day study, none of the treatments exacerbated mortality rates. Instead, they showed varying degrees promoted longevity and reduced the overall MI profiles of traumatized flies (Fig. 5). One of the analogs, CP1, showed a significant enhancement of beneficial effects for adult fly cohorts following mTBI exposure. These *in vivo* results are consistent with the *in vitro* data that CP1 was the most efficacious of the four analogs in cell culture studies. Importantly, the trauma assay indicated that CP1 was more effective than CBN, while the two compounds had very similar profiles in cell-based assays. The improved activity of CP1 in fly trauma studies could reflect multiple whole animal features associated with pharmacokinetics such as drug absorption, distribution and metabolism that are not a part of the cell culture models of oxytosis/ferroptosis. Moreover, the increase in the LPO inhibition of CP1 (Fig. 3) could also contribute to its enhanced protection in mTBI flies. Thus, these results indicate that a combination of *in vitro* cell-based analyses and rapid *in vivo* studies using fly models of neurological disorders is a highly effective approach for evaluating new potential therapeutic compounds in the early-stage drug discovery. Nonetheless, the differences in drug pharmacokinetics between flies and humans necessitate further validation in mammals.

## 5. Conclusions

In the present study, we harnessed a fragment-based drug discovery (FBDD) strategy and generated small molecule libraries comprising the chemical scaffolds that are characteristic of CBN and related phyto-cannabinoids. We systematically screened these fragment chemicals using cell-based phenotypic assays that identify protective effects against oxytosis/ferroptosis and used these results to determine the structure-activity relationship (SAR) of the individual compounds. These data provided fundamental knowledge about the contribution of different chemical structures and functional groups to the anti-oxytotic/ferroptotic activity of cannabinoids. Based on this information, we developed four new CBN analogs that contain key pharmacophores associated with neuroprotection and have improved CNS druglike properties. We subsequently demonstrated that the analogs possess potent neuroprotective activity against oxytosis/ferroptosis by inhibiting lipid peroxidation and mitochondrial ROS, and modulating mitochondrial function in cultured neuronal cell models. Furthermore, we assessed the *in vivo* efficacies of the compounds using a *Drosophila* mTBI model, where one of the four analogs, CP1, was particularly effective. The insights from the FBDD strategy and SAR information unveiled general principles for the rational design of small molecule inhibitors based on CBN for targeting oxytosis/ferroptosis. In addition, the new CBN analogs offer starting points for the development of additional cannabinoid-based drug candidates to treat neurological disorders and metabolic diseases, including cancer, associated with mitochondrial dysfunction. Future studies on the pharmacokinetics and efficacy of the CBN analogs, particularly CP1, using mammalian models of neurological disorders appear warranted.

## CRediT authorship contribution statement

**Zhibin Liang:** Writing – review & editing, Writing – original draft, Visualization, Validation, Supervision, Software, Resources, Project administration, Methodology, Investigation, Funding acquisition, Formal analysis, Data curation, Conceptualization. **Alec Candib:** Writing – review & editing, Methodology, Investigation, Formal analysis, Data curation. **David Soriano-Castell:** Writing – review & editing, Methodology, Investigation, Funding acquisition, Formal analysis, Data curation. **Wolfgang Fischer:** Writing – review & editing, Formal

analysis, Data curation. **Kim Finley:** Writing – review & editing, Methodology, Investigation, Funding acquisition, Formal analysis, Data curation. **Pamela Maher:** Writing – review & editing, Visualization, Validation, Supervision, Resources, Project administration, Methodology, Investigation, Funding acquisition, Formal analysis, Data curation, Conceptualization.

## Declaration of Competing interest

None.

## Data availability

Data will be made available on request.

## Acknowledgments

The work was supported in part by the Paul F. Glenn Center for Biology of Aging Research at the Salk Institute Fellowship (ZL), a Bundy Foundation Fellowship (ZL), a Shiley Foundation Fellowship (DSC), and the National Institutes of Health grants R01AG067331, R21AG064287, R01AG069206, RF1AG061296 (PM) and R21AG067334 (KF). We thank the technical support of the Mass Spectrometry Core of the Salk Institute with funding from NIH-NCI CCSG P30CA01495, NIH-NIA P30AG068635, NIH S10OD021815, and the Helmsley Center for Genomic Medicine. NMR spectra were collected at the UCSD Skaggs School of Pharmacy and Pharmaceutical Sciences NMR Facility.

## Appendix A. Supplementary data

Supplementary data to this article can be found online at <https://doi.org/10.1016/j.redox.2024.103138>.

## References

- [1] WHO, Neurological disorders: public health challenges. <https://www.who.int/publications/i/item/9789241563369>, 2006. (Accessed 1 May 2006).
- [2] S. Gauthier, M. Albert, N. Fox, M. Goedert, M. Kivipelto, J. Mestre-Ferrandiz, L. T. Middleton, Why has therapy development for dementia failed in the last two decades? *Alzheimers Dement* 12 (1) (2016) 60–64, <https://doi.org/10.1016/j.jalz.2015.12.003>.
- [3] I. Bellantuono, Find drugs that delay many diseases of old age, *Nature* 554 (7692) (2018) 293–295, <https://doi.org/10.1038/d41586-018-01668-0>.
- [4] J. Nunnari, A. Suomalainen, Mitochondria: in sickness and in health, *Cell* 148 (6) (2012) 1145–1159, <https://doi.org/10.1016/j.cell.2012.02.035>.
- [5] Z. Liang, A. Currais, D. Soriano-Castell, D. Schubert, P. Maher, Natural products targeting mitochondria: emerging therapeutics for age-associated neurological disorders, *Pharmacol. Ther.* 221 (2021) 107749, <https://doi.org/10.1016/j.pharmthera.2020.107749>.
- [6] M.P. Murphy, R.C. Hartley, Mitochondria as a therapeutic target for common pathologies, *Nat. Rev. Drug Discov.* 17 (12) (2018) 865–886, <https://doi.org/10.1038/nrd.2018.174>.
- [7] S. Tan, D. Schubert, P. Maher, Oxytosis: a novel form of programmed cell death, *Curr. Top. Med. Chem.* 1 (6) (2001) 497–506, <https://doi.org/10.2174/1568026013394741>.
- [8] J. Lewerenz, G. Ates, A. Methner, M. Conrad, P. Maher, Oxytosis/ferroptosis—(Re-) emerging roles for oxidative stress-dependent non-apoptotic cell death in diseases of the central nervous system, *Front. Neurosci.* 12 (2018) 214, <https://doi.org/10.3389/fnins.2018.00214>.
- [9] P. Maher, A. Currais, D. Schubert, Using the oxytosis/ferroptosis pathway to understand and treat age-associated neurodegenerative diseases, *Cell Chem. Biol.* 27 (12) (2020) 1456–1471, <https://doi.org/10.1016/j.chembiol.2020.10.010>.
- [10] D. Soriano-Castell, Z. Liang, P. Maher, A. Currais, Profiling the chemical nature of anti-oxytotic/ferroptotic compounds with phenotypic screening, *Free Radic. Biol. Med.* 177 (2021) 313–325, <https://doi.org/10.1016/j.freeradbiomed.2021.11.003>.
- [11] D. Schubert, D. Kepchia, Z. Liang, R. Dargusch, J. Goldberg, P. Maher, Efficacy of cannabinoids in a pre-clinical drug-screening platform for Alzheimer's disease, *Mol. Neurobiol.* 56 (11) (2019) 7719–7730, <https://doi.org/10.1007/s12035-019-1637-8>.
- [12] Z. Liang, D. Soriano-Castell, D. Kepchia, B.M. Duggan, A. Currais, D. Schubert, P. Maher, Cannabinol inhibits oxytosis/ferroptosis by directly targeting mitochondria independently of cannabinoid receptors, *Free Radic. Biol. Med.* 180 (2022) 33–51, <https://doi.org/10.1016/j.freeradbiomed.2022.01.001>.



- [13] C.W. Murray, D.C. Rees, The rise of fragment-based drug discovery, *Nature Chem* 1 (3) (2009) 187–192, <https://doi.org/10.1038/nchem.217>.
- [14] A. Daina, O. Michielin, V. Zoete, SwissADME: a free web tool to evaluate pharmacokinetics, drug-likeness and medicinal chemistry friendliness of small molecules, *Sci. Rep.* 7 (1) (2017) 42717, <https://doi.org/10.1038/srep42717>.
- [15] W. Fischer, A. Currais, Z. Liang, A. Pinto, P. Maher, Old age-associated phenotypic screening for Alzheimer's disease drug candidates identifies sterubin as a potent neuroprotective compound from Yerba santa, *Redox Biol.* 21 (2019) 101089, <https://doi.org/10.1016/j.redox.2018.101089>.
- [16] L. Huang, D.B. McClatchy, P. Maher, Z. Liang, J.K. Diedrich, D. Soriano-Castell, J. Goldberg, M. Shokhirev, J.R. Yates, D. Schubert, A. Currais, Intracellular amyloid toxicity induces oxytosis/ferroptosis regulated cell death, *Cell Death Dis.* 11 (10) (2020) 828, <https://doi.org/10.1038/s41419-020-03020-9>.
- [17] Z. Liang, B. Zhang, W.W. Su, P.G. Williams, Q.X. Li, C-Glycosylflavones alleviate tau phosphorylation and amyloid neurotoxicity through GSK3 $\beta$  inhibition, *ACS Chem. Neurosci.* 7 (7) (2016) 912–923, <https://doi.org/10.1021/acschemneuro.6b00059>.
- [18] A. Barezat, A. Gonzalez, R.E. Mauntz, R.W. Kotzebue, B. Molina, N. El-Mecharrafie, C.J. Conner, S. Garza, G.C. Melkani, W.J. Joiner, M.M. Lipinski, K.D. Finley, E. P. Ratliff, Using *Drosophila* as an integrated model to study mild repetitive traumatic brain injury, *Sci. Rep.* 6 (1) (2016) 25252, <https://doi.org/10.1038/srep25252>.
- [19] A. Candib, N. Lee, N. Sam, E. Cho, J. Rojas, R. Hastings, K. DeAlva, D. Khon, A. Gonzalez, B. Molina, G. Torabzadeh, J. Vu, K. Hasenstab, K. Sant, J.A. Phillips, K. Finley, The influence of cannabinoids on *Drosophila* behaviors, longevity, and traumatic injury responses of the adult nervous system, *Cannabis Cannabinoid Res* (2023), <https://doi.org/10.1089/can.2022.0285>.
- [20] T.A. Reekie, M.P. Scott, M. Kassiou, The evolving science of phytocannabinoids, *Nat. Rev. Chem* 2 (1) (2017) 101, <https://doi.org/10.1038/s41570-017-0101>.
- [21] X. Luo, M.A. Reiter, L. d'Espaux, J. Wong, C.M. Denby, A. Lechner, Y. Zhang, A. T. Grzybowski, S. Harth, W. Lin, H. Lee, C. Yu, J. Shin, K. Deng, V.T. Benites, G. Wang, E.E.K. Baidoo, Y. Chen, I. Dev, C.J. Petzold, J.D. Keasling, Complete biosynthesis of cannabinoids and their unnatural analogues in yeast, *Nature* 567 (7746) (2019) 123–126, <https://doi.org/10.1038/s41586-019-0978-9>.
- [22] M.J. Waring, Defining optimum lipophilicity and molecular weight ranges for drug candidate - molecular weight dependent lower logD limits based on permeability, *Bioorg. Med. Chem. Lett.* 19 (10) (2009) 2844–2851, <https://doi.org/10.1016/j.bmcl.2009.03.109>.
- [23] R.J. Young, P.D. Leeson, Mapping the efficiency and physicochemical trajectories of successful optimizations, *J. Med. Chem.* 61 (15) (2018) 6421–6467, <https://doi.org/10.1021/acs.jmedchem.8b00180>.
- [24] Z. Liang, Q.X. Li, Discovery of selective, substrate-competitive, and passive membrane permeable glycogen synthase kinase-3 $\beta$  inhibitors: synthesis, biological evaluation, and molecular modeling of new C-glycosylflavones, *ACS Chem. Neurosci.* 9 (5) (2018) 1166–1183, <https://doi.org/10.1021/acschemneuro.8b00010>.
- [25] A.K. Tiwari, M.V. Singh, Insights into the origin and therapeutic implications of benzopyran and its derivatives, *ChemistrySelect* 8 (20) (2023) e202300220, <https://doi.org/10.1002/slct.202300220>.
- [26] J.-F. Uth, F. Borge, K. Lehmkuhl, D. Schepmann, M. Kaiser, V.A.P. Jabor, M. C. Nonato, R.L. Krauth-Siegel, T.J. Schmidt, B. Wunsch, Synthesis and biological evaluation of natural-product-inspired, aminoalkyl-substituted 1-benzopyrans as novel antiparasmodial agents, *J. Med. Chem.* 64 (9) (2021) 6397–6409, <https://doi.org/10.1021/acs.jmedchem.1c00483>.
- [27] Z. Rankovic, CNS drug design: balancing physicochemical properties for optimal brain exposure, *J. Med. Chem.* 58 (6) (2015) 2584–2608, <https://doi.org/10.1021/jm501535r>.
- [28] M. Gao, J. Yi, J. Zhu, A.M. Minikes, P. Monian, C.B. Thompson, X. Jiang, Role of mitochondria in ferroptosis, *Mol. Cell.* 73 (2) (2019) 354–363, <https://doi.org/10.1016/j.molcel.2018.10.042>, e3.
- [29] B. Gan, Mitochondrial regulation of ferroptosis, *J. Cell Biol.* 220 (9) (2021) e202105043, <https://doi.org/10.1083/jcb.202105043>.
- [30] O. Zilka, R. Shah, B. Li, J.P. Friedmann Angeli, M. Griesser, M. Conrad, D.A. Pratt, On the mechanism of cytoprotection by ferrostatin-1 and liprostatin-1 and the role of lipid peroxidation in ferroptotic cell death, *ACS Cent. Sci.* 3 (3) (2017) 232–243, <https://doi.org/10.1021/acscentsci.7b00028>.
- [31] S.A. Mookerjee, A.A. Gerencser, D.G. Nicholls, M.D. Brand, Quantifying intracellular rates of glycolytic and oxidative ATP production and consumption using extracellular flux measurements, *J. Biol. Chem.* 292 (17) (2017) 7189–7207, <https://doi.org/10.1074/jbc.M116.774471>.
- [32] D.A. Ferrick, A. Neilson, C. Beeson, Advances in measuring cellular bioenergetics using extracellular flux, *Drug Discov. Today* 13 (5) (2008) 268–274, <https://doi.org/10.1016/j.drudis.2007.12.008>.
- [33] M. Rabenau, M. Unger, J. Drewe, C. Culmsee, Metabolic switch induced by *Cimicifuga racemosa* extract prevents mitochondrial damage and oxidative cell death, *Phytomedicine* 52 (2019) 107–116, <https://doi.org/10.1016/j.phymed.2018.09.177>.
- [34] V.M. Gohil, S.A. Sheth, R. Nilsson, A.P. Wojtovich, J.H. Lee, F. Perocchi, W. Chen, C.B. Clish, C. Ayata, P.S. Brookes, V.K. Mootha, Nutrient-sensitized screening for drugs that shift energy metabolism from mitochondrial respiration to glycolysis, *Nat. Biotechnol.* 28 (3) (2010) 249–255, <https://doi.org/10.1038/nbt.1606>.
- [35] G. Cheng, R.-H. Kong, L.-M. Zhang, J.-N. Zhang, Mitochondria in traumatic brain injury and mitochondrial-targeted multipotential therapeutic strategies, *Br. J. Pharmacol.* 167 (4) (2012) 699–719, <https://doi.org/10.1111/j.1476-5381.2012.02025.x>.
- [36] B.E. Gavett, R.A. Stern, R.C. Cantu, C.J. Nowinski, A.C. McKee, Mild traumatic brain injury: a risk factor for neurodegeneration, *Alzheimer's Res. Ther.* 2 (3) (2010) 18, <https://doi.org/10.1186/alzrt42>.
- [37] Q. Pang, L. Zheng, Z. Ren, H. Xu, H. Guo, W. Shan, R. Liu, Z. Gu, T. Wang, Mechanism of ferroptosis and its relationships with other types of programmed cell death: insights for potential therapeutic benefits in traumatic brain injury, *Oxid. Med. Cell. Longev.* 2022 (2022) 1274550, <https://doi.org/10.1155/2022/1274550>.
- [38] Q.-S. Li, Y.-J. Jia, Ferroptosis: a critical player and potential therapeutic target in traumatic brain injury and spinal cord injury, *Neural Regen. Res.* 18 (3) (2023) 506–512, <https://doi.org/10.4103/1673-5374.350187>.
- [39] B.R. Stockwell, J.P. Friedmann Angeli, H. Bayir, A.I. Bush, M. Conrad, S.J. Dixon, S. Fulda, S. Gascón, S.K. Hatzios, V.E. Kagan, K. Noel, X. Jiang, A. Linkermann, M. E. Murphy, M. Overholtzer, A. Oyagi, G.C. Pagnussat, J. Park, Q. Ran, C. S. Rosenfeld, K. Salnikow, D. Tang, F.M. Torti, S.V. Torti, S. Toyokuni, K. A. Woerpel, D.D. Zhang, Ferroptosis: a regulated cell death nexus linking metabolism, redox biology, and disease, *Cell* 171 (2) (2017) 273–285, <https://doi.org/10.1016/j.cell.2017.09.021>.
- [40] D. Soriano-Castell, Z. Liang, P. Maher, A. Currais, The search for anti-oxytotic/ferroptotic compounds in the plant world, *Br. J. Pharmacol.* 178 (18) (2021) 3611–3626, <https://doi.org/10.1111/bph.15517>.
- [41] Z. Liang, P. Maher, Structural requirements for the neuroprotective and anti-inflammatory activities of the flavanone sterubin, *Antioxidants* 11 (11) (2022) 2197, <https://doi.org/10.3390/antiox11112197>.
- [42] I.G. Karniol, I. Shirakawa, R.N. Takahashi, E. Knobel, R.E. Musty, Effects of  $\Delta^9$ -tetrahydrocannabinol and cannabidiol in man, *Pharmacology* 13 (6) (1975) 502–512, <https://doi.org/10.1159/000136944>.
- [43] S. Agurell, M. Halldin, J.E. Lindgren, A. Ohlsson, M. Widman, H. Gillespie, L. Hollister, Pharmacokinetics and metabolism of delta 1-tetrahydrocannabinol and other cannabinoids with emphasis on man, *Pharmacol. Rev.* 38 (1) (1986) 21–43, <https://pharmrev.aspetjournals.org/content/38/1/21>.
- [44] A.J. Hill, C.M. Williams, B.J. Whalley, G.J. Stephens, Phytocannabinoids as novel therapeutic agents in CNS disorders, *Pharmacol. Ther.* 133 (1) (2012) 79–97, <https://doi.org/10.1016/j.pharmthera.2011.09.002>.
- [45] N. Hegdekar, C. Sarkar, S. Bustos, R.M. Ritzel, M. Hanscom, P. Ravishanker, D. Philkana, J. Wu, D.J. Loane, M.M. Lipinski, Inhibition of autophagy in microglia and macrophages exacerbates innate immune responses and worsens brain injury outcomes, *Autophagy* 19 (7) (2023) 2026–2044, <https://doi.org/10.1080/15548627.2023.2167689>.
- [46] A. Nordström, P. Nordström, Traumatic brain injury and the risk of dementia diagnosis: a nationwide cohort study, *PLoS Med.* 15 (1) (2018) e1002496, <https://doi.org/10.1371/journal.pmed.1002496>.
- [47] J.L. Marsh, L.M. Thompson, *Drosophila* in the study of neurodegenerative disease, *Neuron* 52 (1) (2006) 169–178, <https://doi.org/10.1016/j.neuron.2006.09.025>.
- [48] S. Lenz, P. Karsten, J.B. Schulz, A. Voigt, *Drosophila* as a screening tool to study human neurodegenerative diseases, *J. Neurochem.* 127 (4) (2013) 453–460, <https://doi.org/10.1111/jnc.12446>.
- [49] U.B. Pandey, C.D. Nichols, Human disease models in *Drosophila melanogaster* and the role of the fly in therapeutic drug discovery, *Pharmacol. Rev.* 63 (2) (2011) 411–436, <https://doi.org/10.1124/pr.110.003293>.
- [50] K. Iijima, H.-P. Liu, A.-S. Chiang, S.A. Hearn, M. Konsolaki, Y. Zhong, Dissecting the pathological effects of human A $\beta$ 40 and A $\beta$ 42 in *Drosophila*: a potential model for Alzheimer's disease, *Proc. Natl. Acad. Sci. U.S.A.* 101 (17) (2004) 6623–6628, <https://doi.org/10.1073/pnas.0400895101>.